CIAMTIS

U.S. DOT Region 3 University Transportation Center

Smart Compaction for Infrastructure Materials

December 31, 2022

Prepared by:

S. Sherand S. Yu

The Pennsylvania State University

r3utc.psu.edu

PennState College of Engineering

LARSON TRANSPORTATION INSTITUTE

Technical Report Documentation Page

1. Report No.	2. Government Accession No.	3. Recipient's Catalog No.
CIAM-COR-R18		

4. Title and Subtitle	5. Report Date
Smart Compaction for Infrastructure Materials	December 31, 2022
	6. Performing Organization Code

7. Author(s)	8. Performing Organization Report No.
Shihui Shen (https://orcid.org/0000-0002-5718-722X) Shuai Yu (https://orcid.org/0000-0002-5947-2155)	LTI 2023-03

9. Performing Organization Name and Address	10. Work Unit No. (TRAIS)
Penn State Altoona 3000 Ivyside Park Altoona, PA 16601	11. Contract or Grant No. 69A3551847103

12. Sponsoring Agency Name and Address	13. Type of Report and Period Covered
U.S. Department of Transportation Research and Innovative Technology Administration 3rd Fl, East Bldg E33-461, 1200 New Jersey Ave, SE Washington, DC 20590	Final Report 6/1/20 – 12/31/22
	14. Sponsoring Agency Code

15. Supplementary Notes

Work funded through The Pennsylvania State University via the University Transportation Center Grant Agreement, Grant No. 69A3551847103.

16. Abstract

Compaction is a process of rearranging material particles by various mechanical loadings to densify the materials and form a stable pavement structure. Current methods to assess the compaction quality rely heavily on engineers' experiences or post-compaction methods at selected spots. The experience-based method is prone to cause compaction problems and pavement distresses, particularly when new materials are implemented. Due to the complicated interactions between the compactors and materials, the compaction mechanism of the particulate materials is still unclear. This gap hinders the improvement of compaction quality and the development of intelligent construction. This project was undertaken to investigate the compaction mechanism of the infrastructure material from the mesoscale (particle scale) and develop an innovative compaction monitoring method that determines the compaction condition based on particle kinematics. With the development of sensing technologies, wireless particle-size sensors have become available in research and industry for monitoring particle behaviors during compaction. A wireless sensor, SmartRock, was applied in the project and collected the mesoscale behaviors during compaction. Several lab and field compaction projects were carried out using asphalt mixtures and granular materials, various compaction machines, and pavement structures. It was found that internal particle kinematic behavior is closely correlated to material densification during compaction. The lab and field compaction can be reasonably connected by the particle rotation, and similar three-stage compaction patterns were identified. Three machine learning models were built to predict the compaction condition and the density of the asphalt pavement both in the lab and in the field. The reasonable predictions confirm that the machine learning algorithm is appropriate for compaction prediction. The density results from the pavement cores further verify the applicability and robustness of the intelligent model for compaction prediction. Future studies are still needed to evaluate the model's robustness based on more mixture varieties and field applications.

17. Key Words	18. Distribution Statement
Asphalt mixture, compaction, machine learning, particle kinematics, sensing technology	No restrictions. This document is available from the National Technical Information Service, Springfield, VA 22161

19. Security Classif. (of this report)	20. Security Classif. (of this page)	21. No. of Pages	22. Price
Unclassified	Unclassified	48	

DISCLAIMER

Table of Contents

List of Figures

List of Tables

CHAPTER 1

Introduction

BACKGROUND

Compaction is one of the most critical steps in roadway construction, which ultimately determines the performance and service life of the pavement [1]. A desirable design of the pavement material could still perform poorly if it has not acquired proper compaction. Linden et al. [2] found that a 1% increase in air voids of asphalt pavement can lead to about a 10% loss of its service life if using 7% as the target air voids, while 3% or fewer air voids could be more likely to have thermal expansion and unstable issues. However, measuring the air voids or compaction condition is tricky, especially in the field. Current approaches to determine the pavement's compaction are mostly based on the engineers' experiences, the density measurement device (e.g., nuclear density gauge and non-nuclear density gauge), and core-taking at selected spots. These post-compaction methods either destroy the unity of the pavement or lack representation of the compaction condition of the whole pavement [3-5]. On the other hand, the calibration of the density gauges is not flexible for different types of pavement structures and material designs. Test sections need to be constructed beforehand to establish the correlations between pavement density and compaction patterns (passes, speed, vibration amplitude, mode, etc.). Once the compaction pattern is determined, the established correlation can hardly be adjusted accordingly. The uniformity and compaction quality along the entire pavement construction cannot be guaranteed.

Intelligent compaction (IC) technology was then invented to collect a variety of real-time field data to supplement engineers' experience and improve compaction quality and uniformity of infrastructure materials. IC technology equips the vibratory rollers with the highly accurate Global Positioning System (GPS), accelerometers, onboard computers, and infrared thermometers for compacted material feedback control [6]. IC technology can collect real-time compaction information at 100% pavement coverage, including the number of rolling passes, surface temperature, and pavement responses. The collected information is displayed on the screen to help engineers to make appropriate decisions so that compaction uniformity can be effectively guaranteed. This technology was initially applied to soil compaction, and the intelligent compaction measurement value (ICMV) shows a consistent correlation with the soil density at its desirable moisture content. However, for other granular materials and multilayer pavement structures, such as asphalt pavement, the correlation between the ICMV and materials density is unstable and inconsistent. The data collected by the IC system are the external responses of the entire structure instead of only a specific layer [7], which is mainly attributed to the inconsistent correlations between the ICMV and the compactability of the granular materials. In addition, the interaction between the granular materials and the roller drums also hinders the establishment of this correlation [7, 8].

Considering the difficulties of using external responses to evaluate pavement compactability, many scholars tried to understand the kinematic and mechanical behaviors of the particulate aggregates during compaction. For the flexible pavement, the mineral aggregates consist of about 95% mass of the asphalt mixture, and most external loads are borne and transmitted by the skeleton of the mineral aggregates. The behavior of the particulate aggregates should be related to the compaction and densification of the materials. How to monitor particle behavior during compaction is the key question to be addressed.

In recent decades, different sensors and devices have been applied in pavement engineering to assess pavement conditions and construction quality. For example, the image acquisition system was used to collect the surface damages and assist the decision-making for pavement management [9]. Fiber Bragg grating (FBG) sensors were frequently used for the long-term performance monitoring of infrastructures in a harsh environment, which is effectively promising compared to conventional strain gauges [10]. Ground penetrating radar (GPR) was applied to detect internal pavement distress according to the propagation and reflection of the electromagnetic wave [11]. The smartphone would collect the external acceleration of the moving vehicle on the pavement to assess the surface roughness of the pavement [12]. These tools can successfully evaluate the conditions of the existing pavements by analyzing the related image or kinematic data at the intermediate temperature. However, the high-temperature condition is still challenging for most of the sensors. The high-temperature environment of the asphalt mixture impeded the application of many devices in compaction research.

SmartRock is a prototype particle-size wireless microelectromechanical system (MEMS) sensor, which has a high survival rate in high- and intermittent-temperature environments. SmartRock has been implemented to research the compaction behaviors of particulate materials and trace the kinematic behaviors of particles during compaction. Wang et al. [4] first introduced the SmartRock in the laboratory compaction and found that the internal particle rotation during compaction strongly correlates with the density of the asphalt mixture. In addition, the particulate materials present different motions and rotations under different types and amounts of compaction efforts, which were used to evaluate the skeleton strength and stability of the structure [13, 14]. The particle rotation during compaction has also proven to be an appropriate indicator of the mixture's workability. The novel evaluation method is sensitive to different mixture designs and compaction conditions [15]. In addition to the particle rotation, the acceleration and contact stress between particles are related to the process of compaction with the aid of the SmartRock sensor. Cheng et al. [16] and Zhang et al. [17] have found that particle contact stress correlates with skeleton formation and mixture densification and can be used to determine the mixture's locking point. The intensity and duration of the particle's acceleration under compaction are also related to the locking condition of the aggregate particles [18]. Other research on the Marshall hammer compaction notes that the intensity and duration of the particle's acceleration respond differently at different compaction stages, which can evaluate the locking condition of the aggregate particles [18]. Compared with the unstable external responses, the internal particle behaviors have been verified to be well correlated with the compactability of the granular materials and multilayer pavement structure. Therefore, the internal particle responses during compaction should be seriously considered and investigated for compaction research.

With advancements in artificial intelligence (AI) and data-sensing technology, the integration of sensors and data-based approaches such as machine learning (ML) have been widely applied in pavement engineering. Researchers have developed various ML models to evaluate pavement roughness and predict its remaining service life. Researchers such as Souza et al. [19], Nabipour et al. [20], and Marcelino et al. [21] developed ML models to evaluate the pavement condition and predict its remaining service life. The reasonable predictions confirmed that ML could be an optimization tool in pavement management systems. Data-based approaches were applied to capture the traffic information in the road network. Kwigizile et al. [22], Amorim et al. [23], and Zhang et al. [24] combined AI and data-sensing technologies and developed different algorithms and neural networks to classify and monitor the types, loads, and speeds of vehicles. The accurate evaluation offered reliable inputs for the pavement structural design. For the more complex performance prediction, ML models and programs can predict the dynamic modulus of asphalt concrete efficiently and accurately. Eleyedath et al. [25] established a novel hybrid ML, and Behnood et al. [26] developed biogeography-based programming (BBP) to predict the dynamic modulus of asphalt concrete. The results from both studies specified that the proposed model offers an efficient and accurate prediction for the dynamic modulus. The ML prediction even outperformed the traditional mechanical models, such as the Witczak and Hirsch models [25, 26]. Given the successful application of machine learning and sensors in engineering, it is a promising and practical way to integrate AI and sensing technology into the

construction of infrastructure materials and help to improve construction quality and achieve more resilient infrastructure.

OBJECTIVES

The compaction mechanism of particulate infrastructure materials has been studied for decades, yet the relationship between the particle level of responses and compaction is still unclear. Such a knowledge gap causes the disconnection between the laboratory and field compaction and hinders the development of more advanced and intelligent compaction technologies. This project undertook to discover the compaction mechanism by understanding the particle kinematic and mechanical behaviors from the mesoscale (particle scale) and establishing a connection between the lab and field compaction. It utilizes an innovative particle-size wireless sensor, the SmartRock, to monitor the particle kinematic behaviors of asphalt mixture and granular materials during compaction.

On the other hand, for the multilayered pavement and granular material compaction, the interaction between the materials and roller compactors is sophisticated, often confounded by many factors such as climate, subgrade condition, and variability in compactors. The second objective of the project is to develop compaction monitoring models that determine the density condition of the asphalt pavement based on particle kinematics. Specifically, it will: (1) identify critical parameters and input variables for compaction prediction of asphalt mixtures and (2) establish intelligent models to predict the compaction condition and density of the asphalt pavement to improve the compaction quality of the asphalt pavement.

CHAPTER 2

Methodology

To achieve the objectives, a wireless MEMS sensor, SmartRock, was used to collect particle behaviors during compaction. With these compaction data, two phases of analysis were conducted: (1) Investigate the compaction mechanism from mesoscale and understand the kinematic and mechanical behaviors of the particle material under the compaction efforts. Both granular materials and asphalt mixtures would be used to investigate the compaction mechanisms under the laboratory and field compaction. (2) Develop an intelligent model based on the compaction mechanism to predict the densification of the pavement. Such models will be built based on AI techniques and ML algorithms. It can predict the compaction condition or the density of the pavement so that a wise decision about the compaction will be made. With the compaction knowledge and prediction model, reasonable compaction strategies can be developed and resilient infrastructure can eventually be constructed. The concept and scope of the proposed work are illustrated in Figure 1.

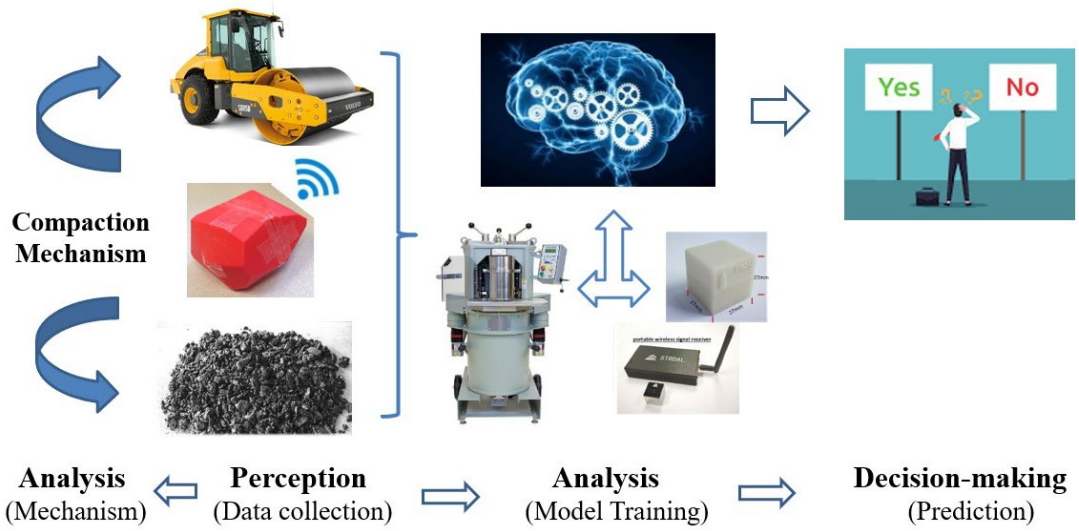

Figure 1. Schematic figure of the research methodology.

CHAPTER 3

Materials and Experiments

MATERIALS

The granular material and asphalt mixture were studied to investigate their compaction mechanism under loadings. The gradation of the granular material is from the Federal Aviation Administration (FAA) Item P209 base material (as shown in Table 1). Eleven asphalt mixtures are included in this study to capture the particle compaction behaviors. These mixtures differ in material type, gradation, mixing methods, compaction temperatures, etc. All mixtures' information and gradation curves are summarized in Table 2 and Figure 2.

Table 1. Gradation of the FAA Item 209 base material.

Sieve Size (in)	Sieve Size (mm)	Design Range	Selected Gradation
2	50	100	100
1-1/2	37	95-100	100
1	25	70-95	87
¾	19	55-85	70
No. 4	4.75	30-60	45
No. 30	0.6	12-30	21
No. 200	0.075	0-8	4

Table 2. Design for the asphalt mixtures.

No.	Technology	NMAS	RAP	OVAC	Asphalt	Temp	Mixing
1	HMA	12.5	15%	5.8%	PG64-22	135 ℃	Plant
2	HMA	9.5	15%	5.9%	PG64E-22	135 ℃	Lab
3	HMA	12.5	0%	5.9%	PG64-22	110 ℃	Lab
4	HMA	12.5	0%	5.9%	PG64-22	143 ℃	Lab
5	0.35% Evotherm	12.5	0%	5.9%	PG64-22	127 ℃	Lab
6	0.7% Evotherm	12.5	0%	5.9%	PG64-22	110 ℃	Lab
7	0.7% Evotherm	12.5	0%	5.9%	PG64-22	143 ℃	Lab
8	Smart Foam	9.5	15%	5.9%	PG64E-22	135 ℃	Plant
9	HMA	12.5	25%	5.9%	PG64-22	135 ℃	Plant
10	Smart Foam	9.5	15%	5.9%	PG64E-22	135 ℃	Plant
11	Foam	9.5	15%	5.8%	PG64S-22	135 ℃	Plant

Note: NMAS means nominal maximum aggregate size; OVAC is the optimal virgin asphalt content; Temp represents the compaction temperature.

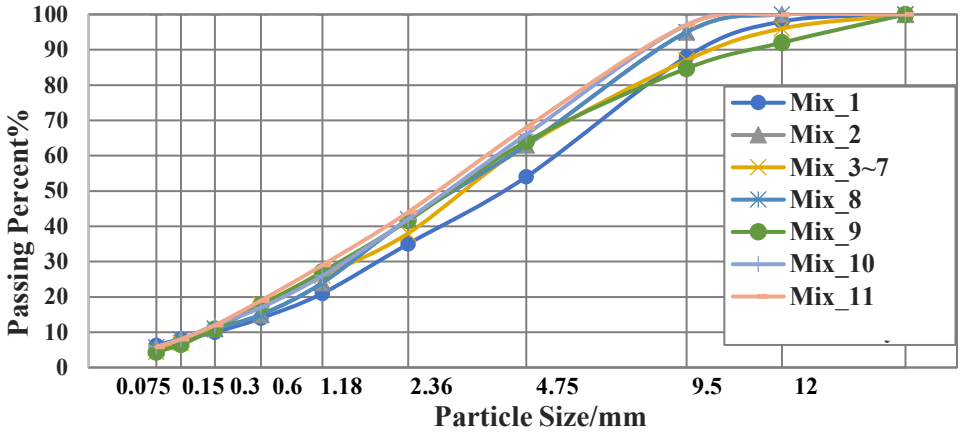

Figure 2. Gradation of the asphalt mixtures.

SMARTROCK SENSOR

SmartRock (Figure 3) is a novel wireless particle sensor. The initial version of SmartRock (Figure 3a) is used in railroad engineering to study the effect of ballast lateral stability [27, 28]. As its size is smaller (Figure 3b), it has been applied in pavement engineering and material compaction [4, 24]. In this project, the SmartRock is a cubic shape with 27 mm length (as shown in Figure 3b). A thermoplastic polymer shell can protect SmartRock from moisture or high-temperature environments up to 150 ℃. SmartRock can record real-time tri-axial acceleration, tri-axial rotation, three-dimensional pressure, and temperature. The sensor and the adaptor are connected and communicated via Bluetooth Low Energy (BLE) technology (Figure 3c) and the data acquisition system in the field (Figure 3d). The compaction data would be simultaneously transmitted to the adapter or computer during compaction. The SmartRock sensor has the "working mode" and "sleep mode" (low energy–consuming mode) to deal with different scenarios. The sleep mode can save a lot of battery power so that the service life can be significantly extended. The sampling frequency of the sensor is also adjustable, and the related information is shown in Table 3. SmartRock has prominent advantages in convenience, durability, reusability, and stability compared to traditional sensors. Its size and wireless data transmission technology reduces disturbances to material movement during data collection. It has been verified by several projects in railway engineering and pavement engineering [4, 24, 27, 28]. Therefore, the SmartRock monitoring system was selected in this study to collect data.

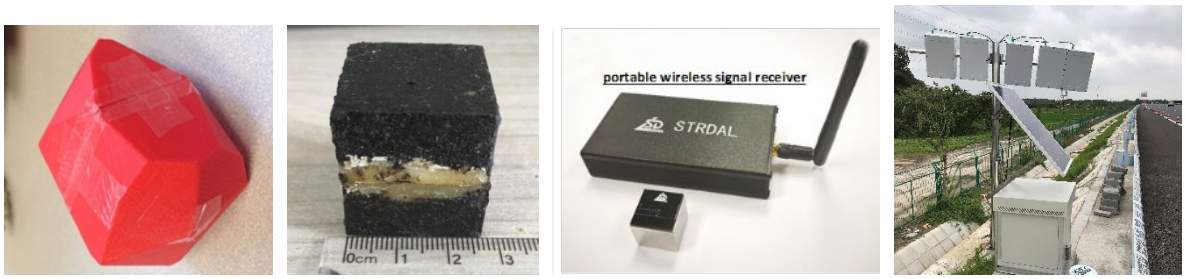

(a) (b) (c) (d)

Figure 3. (a) Initial version of SmartRock with angularity, (b) particle-size SmartRock, (c) SmartRock receiver, and (d) wireless data acquisition system.

Two coordinate systems exist during data collection: local coordinate and global coordinate. To analyze the particle compaction data on the same coordinate, the coordinate transformation matrix would convert the data from the local coordinate to the global coordinate system. The coordinate transformation between global and local coordinates can be achieved by Equations 1 and 2.

$$R = \begin{bmatrix} 1-2(q3^2+q4^2) & 2(q2q3-q1q4) & 2(q2q4+q1q3) \\ 2(q2q3+q1q4) & 1-2(q2^2+q4^2) & 2(q3q4-q1q2) \\ 2(q2q4-q1q3) & 2(q3q4+q1q2) & 1-2(q2^2+q3^2) \end{bmatrix} \quad (1)$$

$$z = R'z' \quad (2)$$

Where $q1$, $q2$, $q3$, and $q4$ are the quaternion from the initial transformation data; z and z' are global and local coordination data, respectively.

Table 3. SmartRock parameters.

Items	Parameters
Size	27×27×27 mm
Weight	43 g
Stress range	1-100 lb
Orientation range	360 °C
Accelerometer	±2 /±4/ ±8/ ±16 g
Gyroscope	±250/ ±500/ ±1,000/ ±2,000 °/s
Magnetometer	± 4,800 uT
Sampling rate	0 ~ 200 Hz
Temperature range	0 ~ 150 °C

LABORATORY EXPERIMENTS

The Superpave gyratory compactor (SGC) is a commonly used compactor in the laboratory. Owing to its internal angle, SGC can apply the shearing loading on the materials to better simulate the real roller compactor loadings. The AFG2 Pine gyratory compactor was utilized in this project. Its calibrated internal angle is 1.15°. The gyration speed is 30 rpm and the compaction pressure is 600 kPa. During compaction, the compactor can collect the compaction loadings, torque, and specimen height so that the compaction energy and resistances can be determined. To collect the particle kinematics during compaction, the SmartRock would be embedded in the center of the materials, since the most stable and representative particle rotation can be collected there [4]. To ensure it is at the center, half of the mixtures are first put in the mold, the SmartRock is then placed on the top and the remaining materials are added. SmartRock would collect the quaternion at a 17 Hz sampling frequency for its stability. To protect the SmartRock from water damage and potential imprecision for data collection, the specimen with the SmartRock cannot soak in the water to measure the density. Therefore, two types of specimens for each asphalt mixture were compacted: (a) **Reference specimen:** one specimen without the SmartRock was compacted to measure the bulk specific gravity (G_{mb}) of the specimen in accordance with the AASHTO T166. (b) **Test specimen:** three specimens with the SmartRock sensor were compacted to investigate the particle compaction characteristics. Each test specimen is deducted by 50 g mass from the G_{mb} of the test specimen to guarantee the same compaction condition as the references. The compaction experiment of the test specimen consists of the following steps:

(1) check the connectivity of the SmartRock with the computer before compaction; collect the initial data on a horizontal platform for the coordinate transformation.
(2) Short-term age the loose mixtures for 2 hours at the desired compaction temperature.
(3) Compact the mixtures and collect the data during the whole compaction process. Meanwhile, the SGC compactor collects the loadings, torque, and height of the compacted specimens.
(4) Extract the SmartRock from the specimen after compaction and allow the sensor to cool down for the next series of tests.

FIELD COMPACTION PROJECTS

Three field compaction projects were carried out to investigate particle behaviors under roller compactions. These projects are different from the pavement structure, asphalt mixtures, design range of equivalent single-axle load (ESAL), etc.

Hollidaysburg Project

The Hollidaysburg project is a maintenance and rehabilitation project for asphalt pavement in Hollidaysburg, Pennsylvania. It is in collaboration with the Pennsylvania Department of Transportation (PennDOT) District 9 office and New Enterprise Stone & Lime Co. Inc. The original pavement was milled 6.35 cm (2.5 inches) from the surface and overlaid with a 2.54-cm (1-inch) leveling course and a 3.81-cm (1.5-inches) wearing course. The wearing course mixture is a PG 64E-22 warm-mix asphalt (WMA) mixture with a nominal maximum aggregate size of 9.5 mm. Detailed information is presented in Table 4. To control the depth of the sensors in the pavement, the SmartRock is manually buried at the bottom of the top layer after the mixtures are placed by the asphalt paver. Static rollers and vibratory rollers were applied to the asphalt pavement. A 17-Hz sampling frequency is used to collect the quaternion of the sensor. A video camera recorded the entire compaction process for verification and analysis. The SmartRock installation and data collection are shown in Figure 4.

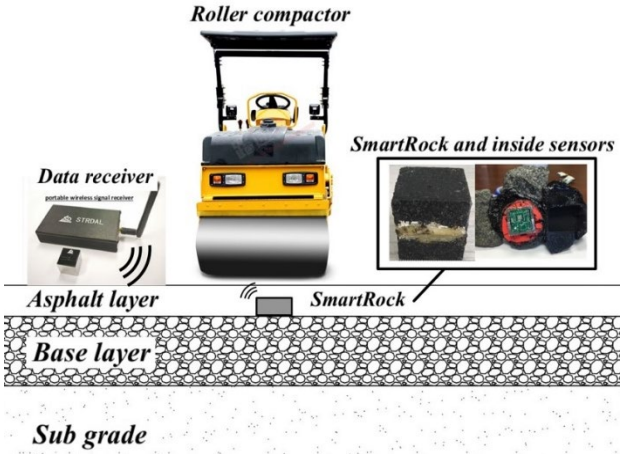

Figure 4. Compaction data collection by the SmartRock system.

Table 4. Information on the asphalt mixtures used for field projects.

	Hollidaysburg Project	Altoona Project	Indiana Project
Mixture type	WMA9.5	WMA9.5	HMA12.5
Virgin binder	PG 64S-22	PG64E-22	PG 64-22
Virgin binder content	5.2%	5.1%	4.7%
RAP content	15%	15%	25%
Total binder content	6.1%	5.9%	5.9%
Theoretical max specific gravity	2.480	2.469	2.496
Gyration at N_{design}	75	100	50

Altoona Project

The Altoona project is a maintenance and rehabilitation project for asphalt pavement in Altoona, Pennsylvania. The original pavement was milled 6.35 cm (2.5 inches) from the surface and overlaid with a 2.54-cm (1-inch) leveling course and a 3.81-cm (1.5-inches) wearing course. The mixture design of the wearing course is presented in Table 2, No. 8, and detailed information is provided in Table 4. SmartRock was manually buried at the bottom of the top layer for data collection. Eleven compaction cycles were applied to the asphalt pavement, including static roller and oscillatory roller (HD+ 120i VO Tandem Roller, as shown in Figure 5). The parameters of the oscillatory roller are presented in Table 2, and the oscillation frequency of this compactor is 36 Hz. The sampling frequency was set at 17 Hz and 100 Hz for collecting quaternion and acceleration, respectively. To investigate the relationship between the external and internal pavement responses, an accelerometer was fixed on the shaft of the vibratory roller to capture the acceleration during compaction (Figure 5). The sampling frequency of the accelerometer was 400 Hz. A camera also recorded the whole compaction process for the subsequent verification and analysis. SmartRock installation and data collection are shown in Figures 5 and 6.

Figure 5. Roller compactor and SmartRock on the drum.

Figure 6. SmartRock installation and data collection during compaction in the Altoona project.

Indiana Project

The Indiana project is a newly constructed asphalt pavement in Angola, Indiana. The asphalt mixture used in this project is HMA-12.5 and detailed information is shown in Table 4. The target depth of the asphalt layer was 5.08 cm (2 inches). SmartRocks are buried at the bottom of the asphalt layer to collect the internal particle responses. Both static roller and vibratory roller (as shown in Figure 7) were applied for compaction. The same sampling frequencies of 17 Hz and 100 Hz were selected to collect the particle rotation and translation, respectively. An accelerometer with a 400-Hz sampling frequency was fixed on the vibratory rollers to collect the external responses. After the compaction, two core samples near the SmartRock were drilled out to measure the density of the pavement. The SmartRock installation and data collection are shown in Figure 8.

Figure 7. Vibratory roller in Indiana project and the SmartRock on the roller.

Figure 8. SmartRock installation and data collection in the Indiana project.

CHAPTER 4

Compaction Mechanism

In this section, the particle kinematic behaviors, including the internal particle rotation and translation, and the external pavement responses, will be monitored by the SmartRock sensor. The compaction mechanism of the granular materials and asphalt mixture will be investigated under various compaction methods and conditions.

GRANULAR PARTICLE KINEMATICS UNDER COMPACTION

Particle Rotation and Density

Compaction is a process of particulate material rearranging and consolidating in response to external mechanical forces (energy). The kinematic and mechanical properties of the mixture particle would present differently at different compaction stages. The correlations between the compactability and responses (external and internal) of the asphalt pavement were both studied by previous research. The external responses were collected and analyzed by IC technology. Because of the multilayered structure of the asphalt pavement, the external responses from the entire pavement structure are hardly related to the compactability of the sole asphalt layer. Comparably, the internal particle responses can represent the compaction behaviors of the asphalt material. With the aid of the SmartRock sensor, Wang et al. [4] found that the mixture particles rotated at a consistent period as the SGC compactor. Its cycle period is 2 seconds, which is consistent with the gyration patterns of SGC. In addition, the amplitude of the Euler angle is also different at various compaction stages. The amplitude decreases as the compaction proceeds, and the material becomes denser and stiffer. Based on that, the relative rotation was defined, which is the difference between the peak and the valley value in a single cycle (Figure 9).

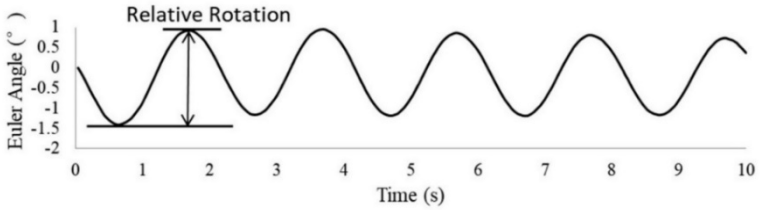

Figure 9. Illustration of the relative rotation [4].

Plotted in Figure 10 is the relative rotation curve of the FAA item P209 base material. Only 20 gyrations were conducted in case of breaking aggregates. It is worth noting that these two curves are similar in trend. The relative rotation is not smoother for lacking lubrication, but the relative rotation curve is still around the curve of the specimen height. Given the constant mass of the specimen during compaction, the height is also an indicator of the specimen density. The consistent trend between the particle's relative rotation and the height change of the specimen indicates that the relative rotation is highly related to the mixture's densification during compaction.

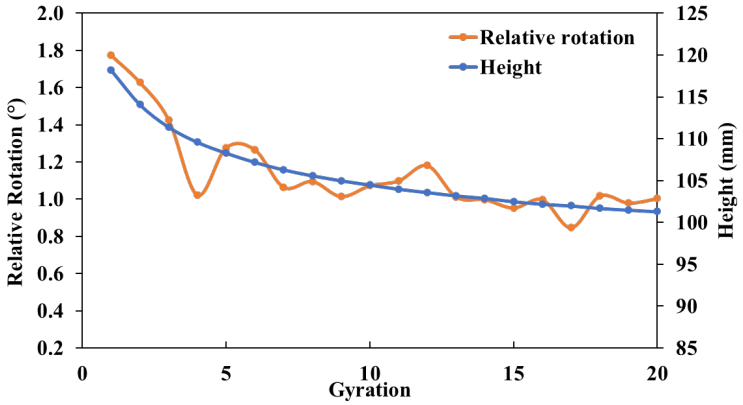

Figure 10. Comparison between relative rotation and specimen height for granular material compaction.

Particle Rotation and Moisture Content

The base material with the same gradation (as shown in Table 1) but various moisture contents was studied to investigate the effect of moisture on particle rotation during compaction. The optimum moisture content was first determined based on the standard protocol test. For the protection of the coarse aggregates and the limited water absorption of the coarse aggregates, aggregates larger than 4.75 mm were first sieved out and the rest of the materials were used to do the protocol test. The results are presented in Table 5 and Figure 11. The optimum moisture content for the granular material is 3.6%.

Table 5. Determination of the optimum moisture content.

Test No.	Wet sample + Mold (g)	Mold (g)	Wet sample (g)	Volume (cm^3)	Moisture content (fine)	Moisture content (entire)	Dry Unit Weight
1	6,261.1	4,205.5	2,055.6	2,127	3.80%	1.70%	0.931
2	6,315.5	4,205.5	2110	2,127	4.70%	2.10%	0.948
3	6,403.9	4,205.5	2,198.4	2,127	6.50%	2.90%	0.971
4	6,471.9	4,205.5	2,266.4	2,127	8.30%	3.70%	0.984
5	6,403.1	4,205.5	2,197.6	2,127	10.10%	4.50%	0.939

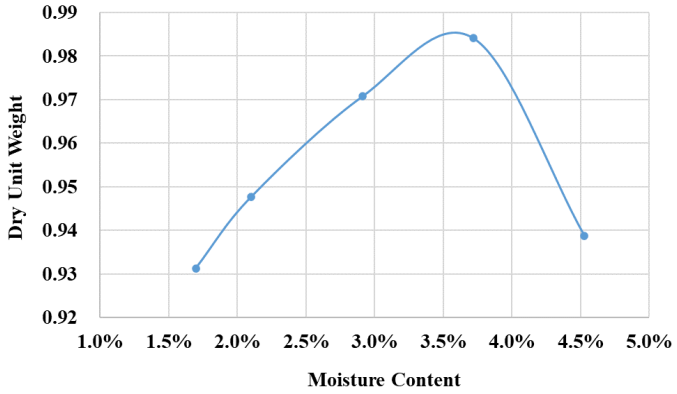

Figure 11. Determination of the optimum moisture content.

The granular material with a 2% and 4% moisture content was compacted in the study. To avoid cracking the aggregates, only 20 gyration cycles were applied to the materials. Two replicate samples for each scenario were compacted, and the average relative rotation curve was presented in Figure 12. It is worth noting that the relative rotation for the two curves is similar in trend and magnitude. The changing of the relative rotation is related to the densification of the material. At the beginning of the compaction, the relative rotation is large and the decrease is rapid, which is related to the dramatic particle rotation and material densification. Afterward, the relative rotation is stable with some variations, which is due to the rearrangement of the aggregate particles and the material's further densification. The similarity of the two curves indicates that under the moisture content of 2% and 4%, the water did not make obvious effects on the compactability of the granular material. The conclusions are based on the limited compaction experiments with two moisture contents. More experiments about the granular materials or asphalt mixtures are needed to verify these findings.

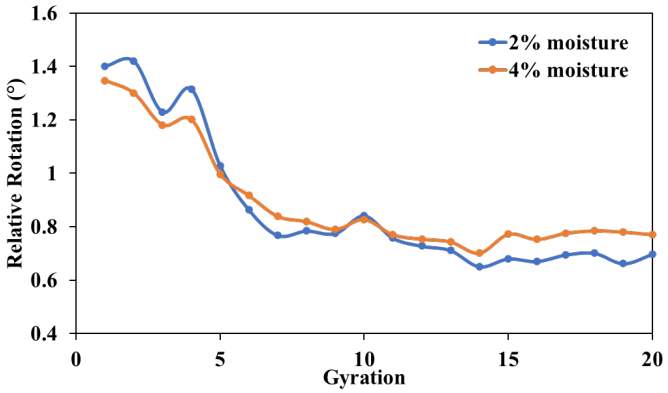

Figure 12. Relative rotation at different moisture contents for granular material compaction.

ASPHALT PARTICLE KINEMATICS UNDER LABORATORY COMPACTION

Particle Rotation and Density

To investigate the compaction mechanism of other particulate materials, the same gyratory compaction was also performed on the asphalt mixture. The relative rotation curve (the orange curve in Figure 12) depicts the compaction process of the asphalt mixture. At the beginning of the compaction (stage I, breakdown stage), asphalt mixture particles were loose and had limited contact. The shear and compression forces of SGC started to cause particles to rotate and coalesce. Particles had large relative rotation and a sharp reduction due to much compaction and height (density) reduction. After transitioning into stage II (main compaction stage), particle movement was restricted, as represented by the reduced relative rotation rate. However, compaction continued, resulting in further specimen height reduction. Starting from stage III (finishing stage), particle rotation was much restricted by the compacted structure, except following the regular rotation of the gyratory compactor. A very minimal height (density) change was further achieved. In other words, the mixture practically entered a locking point where most particles interlocked; additional compaction effort could have a very limited impact on density change. Compaction is most effective during the first and second stages. After the particles stabilize with constant relative rotation, the compaction approximates completion. The further increasing number of gyrations generally couldn't change the air void of the specimen because the particles have been interlocked, preventing them from additional relative rotation.

Also plotted in Figure 13 is the height curve (blue curve) of the same mixture during compaction. It is worth noting that the height change of the specimen follows a similar trend. At the beginning of the compaction, the specimen was rapidly compacted because of the loose mixture properties, resulting in a

larger height decrease. Then the particles contact each other, and the increased shearing stress hinders further compaction, and the height decreases at a low rate and eventually reaches the end of the compaction. The consistent trend between the particle relative rotation and the height change of the specimen indicates that the relative rotation is highly related to the mixture's compaction; since the mass of the mixtures keeps unchanged, the height here is the same concept as the density and compactability of the asphalt mixture. Therefore, the particle kinematic behavior (particle rotation) is closely related to the mixture's density and could be used in the compaction prediction.

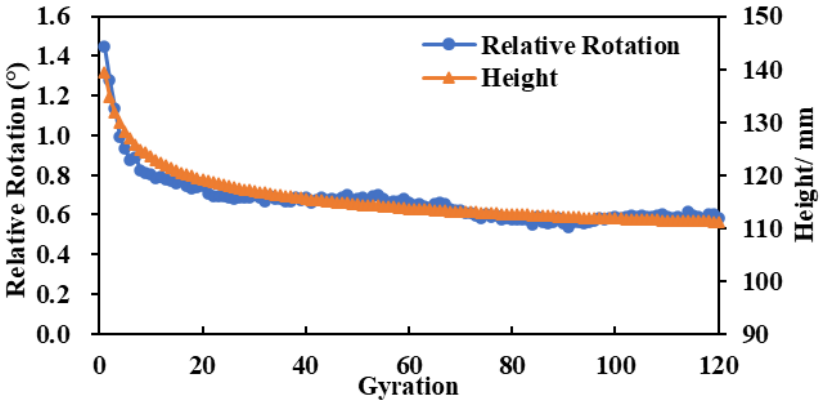

Figure 13. Comparison between relative rotation and specimen height for asphalt material compaction.

Particle Rotation and Asphalt Content

The asphalt mixture with the same gradation (as shown in Table 2, No. 2) but various asphalt contents was studied to investigate the effect of asphalt content on particle rotation during compaction; 5.2% and 6.0% asphalt content and three replicate samples for each scenario were compacted. To clarify, 6.0% asphalt content is the optimum asphalt content (OAC) for the mixture design; 5.2% asphalt content was compacted for the research. The average relative rotation curve is presented in Figure 14. It is worth noting that the relative rotation for two types of asphalt mixtures is similar in trend, which is consistent with the compaction theory, as elaborated in the last section. However, the magnitude of the relative rotation is affected by the asphalt content. More asphalt content results in a larger particle rotation during compaction. This conclusion is consistent with the engineering experience that asphalt acts like a lubricant to assist the aggregate bonding and to rotate under the compaction loadings.

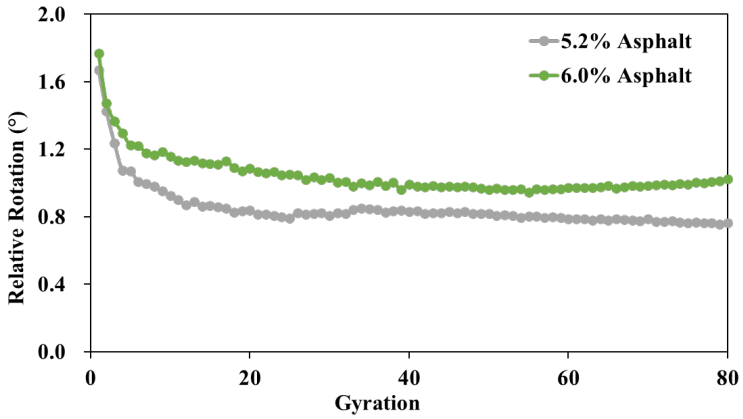

Figure 14. Relative rotation at different asphalt content for asphalt material compaction.

Particle Rotation and Compaction Temperature

The asphalt mixtures with the same gradation (as shown in Table 2, mixtures No. 3 and No. 4) have been compacted at different temperatures to investigate the effect of temperature on particle rotation. Three replicate samples for each scenario were compacted. The average relative rotation curve is presented in Figure 15. As seen, the compaction temperature affected the particle rotation during compaction. Low-temperature environment results in a smaller particle rotation, which is consistent with the engineering experience. Asphalt is the lubricant in asphalt mixture, low temperatures cause it to be thicker and more viscous, and that will prevent the particle rotation and compaction of the asphalt mixture.

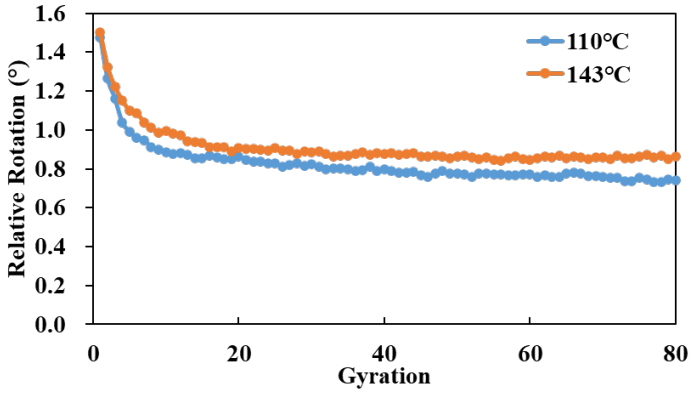

Figure 15. Relative rotation at different compaction temperatures for asphalt material compaction.

Particle Rotation and WMA Additive

Tests of the asphalt mixture with the same gradation (as shown in Table 2, mixtures No. 3 and No. 6) but different content of WMA additive were carried out to investigate the effect of WMA additive on particle rotation. The additive used here is a chemical additive, Evotherm M1. It can improve the coating of aggregates by reducing the surface energy of the aggregate/binder interface and the inner friction. Three replicate samples for each scenario were compacted. The average relative rotation curve is presented in Figure 16. It is worth noting that the relative rotation for two types of asphalt mixtures is similar, but the magnitude of the relative rotation is affected by the WMA additive. It is clear that the additive can increase the particle rotation compared with the virgin mixture (with 0% additive). Therefore, the WMA additive can improve the particle rotation and property of workability.

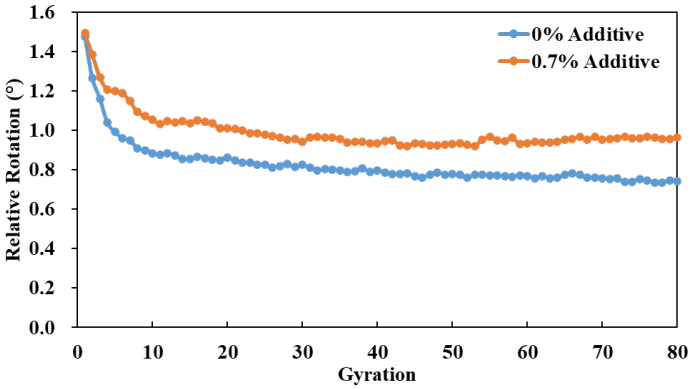

Figure 16. Relative rotation for different content of WMA additive for asphalt material compaction.

Comparison between Laboratory and Field Compaction

Besides laboratory compaction, field compactions have also been conducted to investigate the compaction mechanism. The same asphalt mixture (No. 10 in Table 1) was used in both lab and field compaction. Figures 17 and 18 present the particle rotation observed under the gyratory and roller compactors. Under the vertical compaction loadings, the particle rotation presents higher values in the horizontal direction than in the vertical direction, regardless of the compaction method. It is noted that the general trend of the particle kinematic behaviors through the compaction process followed a similar three-stage pattern for these two methods:

Stage I (breakdown stage): lab compaction (1st to 7th gyration) and field compaction (1st and 2nd cycle). This stage is short, but the most dramatic rotation and speedy decrease occur during this stage while the properties of the asphalt mixtures are loose. The fastest material densification also occurs in this stage. Stage II (main compaction stage): lab compaction (8th to 50th gyration) and field compaction (3rd to 8th cycle). Coarse aggregates begin to contact each other and form the skeleton. This stage is characterized by the imbalanced interaction between compaction loadings and particle shearing resistances. Most material densification occurs in this stage but at a relatively low speed. Stage III (finishing stage): lab compaction (after the 50th gyration) and field compaction (after the 8th cycle). The particle rotation is relatively stable and the interaction between compaction loadings and particle resistance reaches balance at this stage. Minimal densification but surface leveling occurs in this stage.

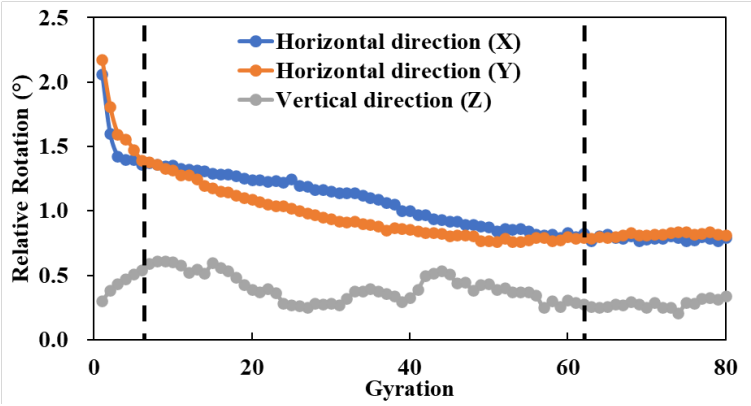

Figure 17. Particle rotation curve under gyratory compaction for the Altoona project.

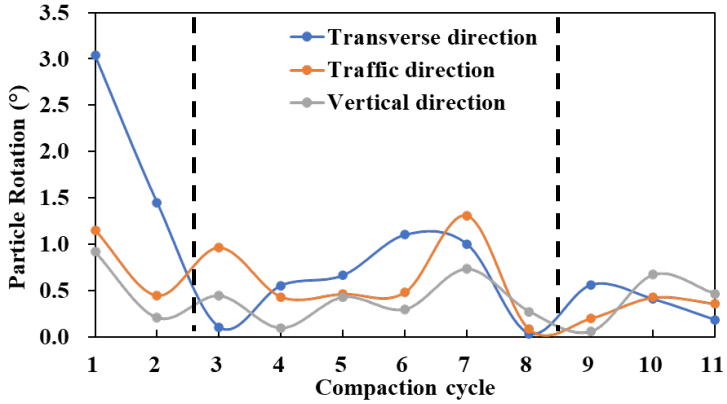

Figure 18. Particle rotation under roller compaction for the Altoona project.

Particle Translation During Compaction

The particle kinematic behavior was analyzed based on the Altoona field project. The peak-peak acceleration is used in this section for analysis, which is the difference between the maximum and minimum acceleration under a single compaction cycle. Different compaction efforts have been identified based on the recorded video. As seen in Figure 19, the largest acceleration of the particles occurs during the 1st to 3rd and 7th to 9th cycle in the traffic direction. These cycles are compacted by the oscillatory roller, which can generate horizontal vibrations to knead and compact the materials. For the 4th to 6th cycle and the last two cycles, the vertical acceleration presented the largest value of the three directions. These responses are from the static roller, which uses its drum gravity to compact the pavement. By comparing the particle responses of these two compactors, it affirms that the vibratory mode of compaction is much more effective than the static mode.

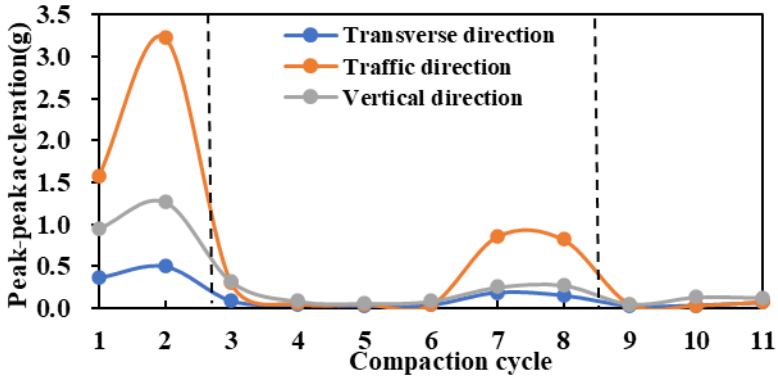

Figure 19. Internal particle acceleration for the Altoona project.

Figures 19 and 20 present the acceleration responses from the vibratory roller and the static roller, respectively, for two field projects. To clarify, these two projects used different designs of roller compaction. For the Hollidaysburg project in Figure 20, static compaction was applied at the beginning of the compaction and followed by vibratory compaction. Comparably, the static compactions are applied between the vibratory compactions for the Altoona project in Figure 21. Comparison between these two scenarios demonstrates the effect of compaction sequences on the compactability of asphalt pavement.

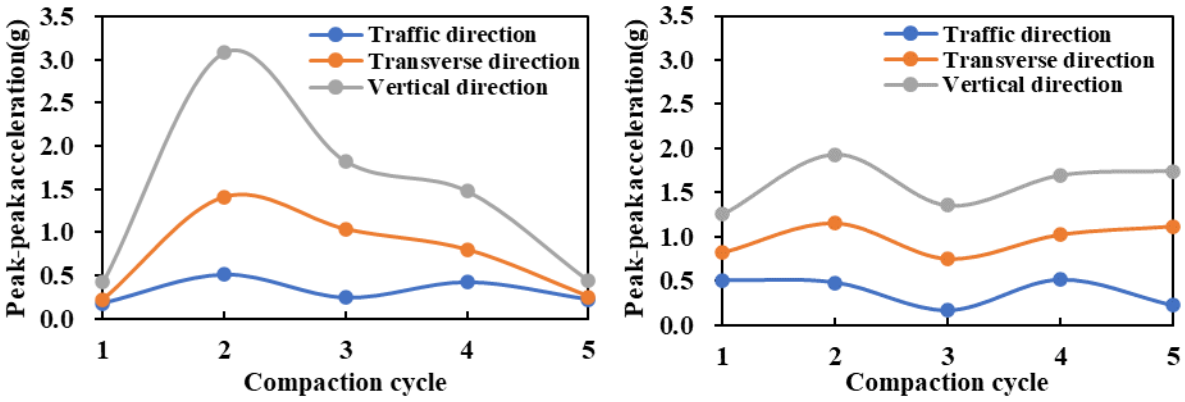

Figure 20. Internal acceleration of the Hollidaysburg project under (a) vibratory roller compaction and (b) static roller compaction.

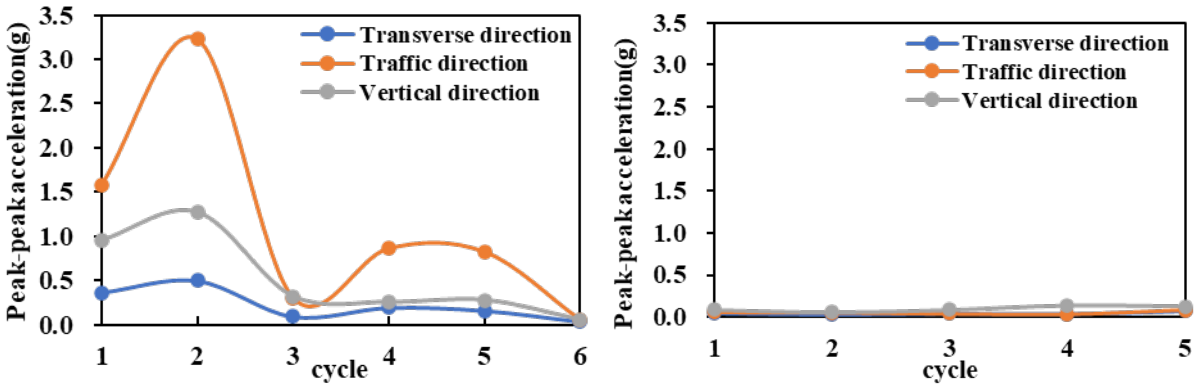

Figure 21. Internal acceleration of the Altoona project under (a) vibratory roller compaction and (b) static roller compaction.

When the static rollers were performed at the beginning of the compaction, the particles' responses were more active (Figure 20b) than those applied after the vibratory compactions (Figure 21b). For the latter scenario in Figure 21, the static compaction has a minimal compaction effect. The responses under the static compactions don't show many fluctuations, which affirms that static compactions contribute to the surface smoothing instead of material densifications.

Comparatively, the responses under the vibratory roller were not affected by the design of the compactions. As seen in Figure 20a and Figure 21a, the vibratory responses are similar even though different designs of vibratory compactions were applied in the two projects. In the beginning, for the loose status of the asphalt material, the particle moves limitedly under vibratory loadings (first cycle). As more compaction energies were applied, the formed skeleton and the connected stress chains resulted in dramatic particle motion in the second cycle. In addition, the shearing resistance gradually developed between particles, which caused the decrease of the particle motion afterward and eventually entered static at the end of the compaction. It's also worth noting that the particle responses at the 3rd cycle present distinctions between the two projects. This phenomenon might be because of the interaction between the compaction energy and particle shearing resistances. Based on the compaction theory of granular materials, the transition between the jamming condition to dynamic compaction results in motion variations. This transition usually occurs at the main compaction stage (from the 3rd to the 5th cycle). The variations of the particle behavior are related to the particle's engineering properties, the amount and intensity of the compaction energy, etc. [29].

PAVEMENT RESPONSES AND ASPHALT COMPACTABILITY

Concept of ICMV

The external acceleration was originally analyzed in soil mechanics to assess the compaction quality [30, 31]. When the roller compactor is applied to the soft or uncompacted soil, the external responses collected on the roller are simple, and the energy is mainly distributed at the dominant (fundamental) frequency. As the soil becomes denser and stiffer, the response from the compacted materials becomes complex, and the energy is scattered at several frequencies, which are integral multiples of the dominant frequency [8]. A linear relationship between compaction meter value (CMV) and compaction control value (CCV) and materials' stiffness is identified, especially when the soil is at the optimum water content [3]. Based on this theory, Equations 3 and 4 are proposed to determine the compactability of the compacted materials [31]. Since the acceleration is initially collected in the time domain, a discrete Fourier transform is used to convert the acceleration from the domain of time to frequency. In this study, CMV and CCV were

used to quantify the compactability of the asphalt pavement based on the external responses collected by the accelerometer on the compactor drum in the Altoona project.

$$CMV = 300 \times \frac{A_{2\Omega}}{A_{\Omega}} \tag{3}$$

$$CCV = 100 \times \frac{A_{0.5\Omega}+A_{1.5\Omega}+A_{2\Omega}+A_{2.5\Omega}+A_{3}}{A_{\Omega}+A_{0.5\Omega}} \tag{4}$$

Where $A_{i\Omega}$ means the amplitude of the i multiplies the dominant frequency.

Figure 22 shows the traffic-direction acceleration in the domain of time and frequency, respectively. The analysis was focused on the traffic direction, since oscillatory rollers generated the most significant vibration in the traffic direction. It is roughly axisymmetric by the 0-horizontal line and the peak acceleration is about 2 g (1 g = 9.8 m/s). The fast Fourier transform (FFT) is then performed, and the frequency-domain responses are shown in Figure 21b. After matching the time tags of the SmartRock and the accelerometer, six cycles of oscillatory compaction at the same location are selected. Considering the effective zone of the oscillatory roller, 4 seconds of acceleration data is used for the FFT analysis. In the frequency domain (Figure 21b), several frequencies have much stronger intensities than others, which centralize the most compaction energies. These spikes occur at around 36 Hz, 72 Hz, 108 Hz, etc., which are consistent with the dominant frequency of the oscillatory compactor.

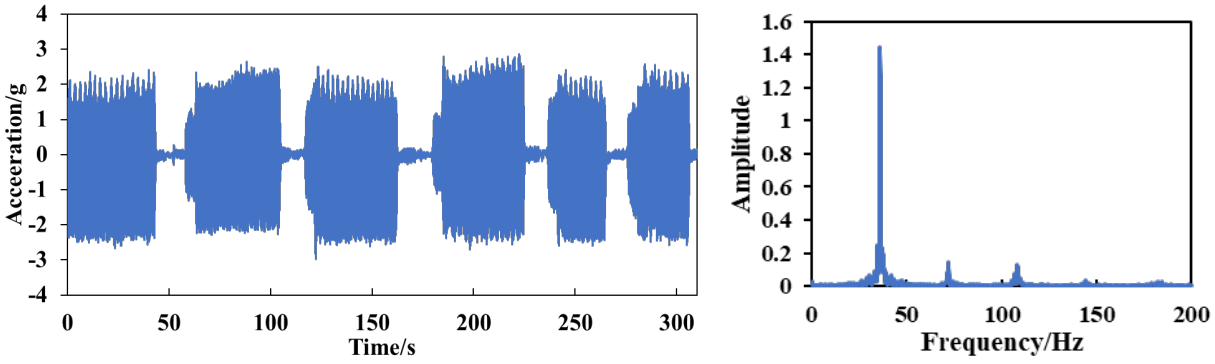

(a) (b)

Figure 22. External acceleration in the domain of (a) time and (b) frequency.

Correlation between Pavement Responses and Compactability

Figure 23 compares the internal and external responses during compaction. To clarify, the internal particle responses were collected by the SmartRock sensor inside the pavement, while the external responses were collected by the accelerometer on the roller drum. The external response of the first cycle is not collected for practical reasons. It is worth noting that particle acceleration is related to material property and densification. The internal responses have been explained in the last section in Figure 21a. It shows the three compaction stages, and the change of the particle acceleration results from the material properties and densification. Comparably, the ICMV does not present a clear distinction at three stages. The ICMV increases first and reaches the peak in the 3rd cycle, which might be because the material became denser under compaction. The curve then decreases and maintains a relatively constant value. After comparison, the peak for ICMV occurs in the middle of the compaction.

Solid conclusions cannot be made only based on the ICMV, which might be related to the influence depth of the vibratory roller, different support conditions, and the high damping ratio of the asphalt material. Some other factors, such as the changing temperature and the variation of the IC machines, would also affect the correlation. A certain relationship between the ICMV and the internal particle responses remains to be uncovered. Combining the previous findings about the ICMV, it's not recommended to evaluate the

compactability of asphalt pavement solely based on external responses. Jointly considering the internal and external responses is a more appropriate method for the quality control of asphalt compaction.

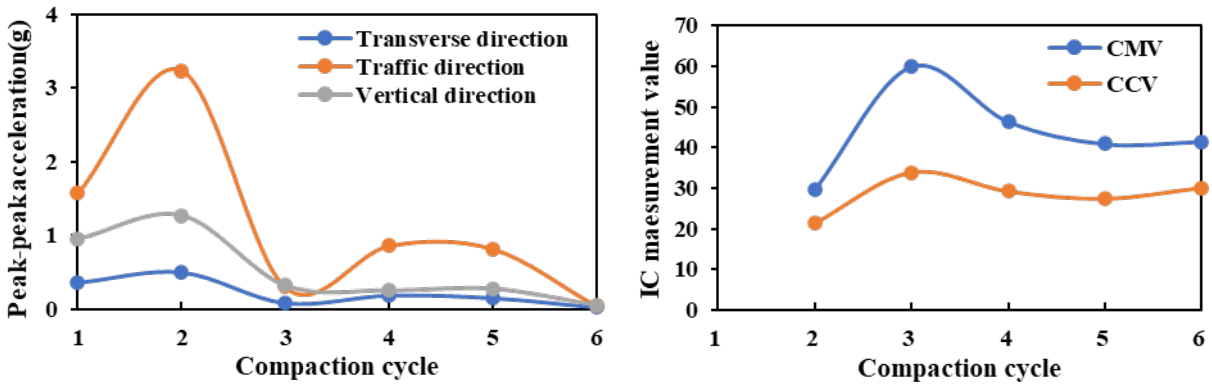

(a) (b)

Figure 23. Comparison between (a) internal responses and (b) external responses for the Altoona project.

CHAPTER 5

Prediction Model Development

In this chapter, compaction prediction models are established based on the findings of the compaction mechanism. The model development includes the input variable selection, the output determination, and the algorithm selection for different predictive models.

INPUT VARIABLE SELECTION

Three parameters are investigated for their relationships with material densification. These three parameters are (1) particle kinematic behavior (particle relative rotation), which is collected by the SmartRock sensor; (2) mechanical parameter, which is recorded by the gyratory compactor; and (3) compaction energy applied to the paved materials. The definition of the particle relative rotation and the correlation between the particle rotation and the material density have been elaborated in Chapter 4. The other two parameters will be introduced below.

Mechanical Parameter

The compaction of the asphalt mixture is influenced by the contact and interlocking behaviors between aggregates [32]. The mechanical properties between particles were related to the particle rotation and interlocking during compaction, as well as the workability of the asphalt mixture. Compaction densification index (CDI), compaction force index (CFI), and normalized shear index (NSI) are the most common mechanical parameters to evaluate the workability of asphalt mixtures [33]. Because the CDI is calculated from the $\%G_{mm}$ and the $\%G_{mm}$ was for determining the compaction condition in this study, CDI is not suitable for the input of the model. CFI indicates how much resistive effort it overcame to compact the mixtures from the initial cycle to 92% G_{mm}, as shown in Figure 24. The resistive effort W is defined in Equation 5 [33]. NSI represented the work applied by the compactor to resist the frictional shear during compaction. In calculating the shear frictional resistance, it assumes the sample is fully constrained at any gyration and the energy due to surface traction is negligible [33]. The NSI can be known according to the conservation of energy by Equation 6.

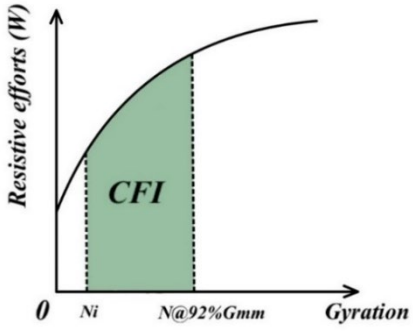

Figure 24. Illustration of CFI.

$$W = \frac{4ePθ}{Sh} \quad (5)$$

$$\tau = \frac{M+PShθ}{V} \quad (6)$$

Where S is the section area of the specimen, V is the volume of the specimen, θ is the tilting angle of the compactor, and is the same as the shear strain γ. Other notations can be found in Figure 25.

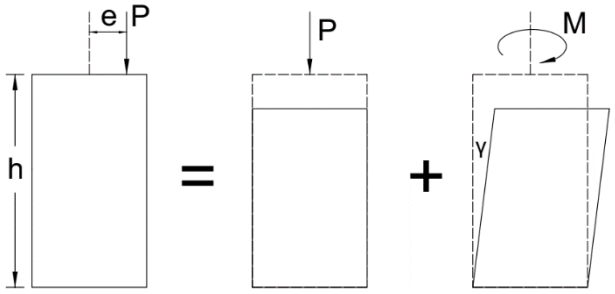

Figure 25. Schematic diagram of the SGC compaction.

Compaction Energy

For the infrastructure material compaction in the lab and field, three compactors have been commonly used in practice and are also adopted in this research. They are the Superpave gyratory compactor (SGC), static roller compactor, and vibratory roller compactor. The determination of the compaction energy applied by these three compactors is explained below.

The SGC can impart vertical loadings and constant shear forces throughout the asphalt mixture sample. The introduction of the gyration angle generates both shearing and kneading effects on the asphalt mixtures. Therefore, the total gyratory compaction energy per unit mass is the sum of the energy due to the vertical loading force (E_1) and the moment by the eccentricity of the applied force (E_2), as determined in Equation 7 [34].

Vibratory rollers can apply two types of compaction effort: the static weight by the weight of the drums and the frame and the dynamic impact force by a rotating eccentric weight located concentrically to the drum. The weight of the roller, compaction speed, and vibration condition (i.e., the frequency and amplitude of the vibration) would impact the compaction energy of the vibratory roller to the asphalt pavement. The compaction energy of the vibratory roller compactor per unit mass per compaction cycle can be determined based on Equation 8 [35]. The information on the vibratory rollers used for the two projects is presented in Table 6.

The static roller uses its weight to compact the materials or level the surface at the beginning or finishing compaction. The weight of the static roller is the key factor in its compaction energy, which is determined based on Equation 9 [36]. The compaction energy of the static roller is also affected by the rolling resistance coefficient, which is determined based on the interaction material and the compaction process. For the asphalt pavement compaction project in Altoona, the static roller is used in the middle and end of the compaction. Based on the literature, 0.09 and 0.05 are selected as the rolling resistance coefficient for the middle and finishing phases, respectively [36].

$$E = E_1 + E_2 = \frac{P*S*\Delta h}{m} + \frac{4\pi*\theta}{m}\sum M_i \quad (7)$$

$$E_v = \frac{f}{v\rho hb} * 2A * (Rg + \frac{\pi F_e}{4}) \quad (8)$$

$$E_s = c * \frac{Rg}{\rho hb} \quad (9)$$

Where ***P*** is the applied vertical force, ***S*** is the section area of the specimen, ***θ*** is the tilting angle, ***M*** is the moment by the eccentricity of the applied force, and ***m*** is the mass of the material. ***C*** is the rolling resistance coefficient**,** ***h*** is the depth of the material, ***b*** is the width of the roller drum, ***A*** is the amplitude of the roller vibration, ***f*** is the vibratory frequency, ***Fe*** is the centrifugal force of the roller, ***v*** is the speed of the roller, and ***R*** is the mass of the roller.

Table 6. Information on the vibratory rollers.

Machine Parameters	Altoona Project	Indiana Project
Frequency (*f*)	42 Hz	45 Hz
Speed (*v*)	1.3 m/s	0.7 m/s
Density (*ρ*)	2,370 kg/m^3	2,372 kg/m^3
Width (*b*)	1.98 m	1.8 m
Amplitude (*A*)	0.88 mm	0.84 mm
Weight (*m*)	12.2 t	18 t
Centrifugal force (*Fe*)	159 KN	214.9 KN

OUTPUT DETERMINATION

The Superpave gyratory compactor (SGC) is used to compact the asphalt mixture in the laboratory. During the compaction, the Pine G2 SGC compactor monitored the compaction loading, torque, and height of the specimen at each gyration. The density or %Gmm of the specimen at each gyration can be determined by Equation 10. For the field compaction, it is impractical to measure the density during the compaction. The pavement density would be measured after compaction by the core samples taken from the pavement and be used to verify the model prediction. Three dataset scenarios are also conducted to verify the robustness of machine learning models.

(1) Scenario I: All compaction data serve as the training dataset to establish the model and test the prediction accuracy.
(2) Scenario II: 70% of random compaction data serves as the training dataset, and the rest of the 30% of data points serve as the test dataset.
(3) Scenario III: Eight mixture compaction data points are used to train the model, and the rest of the three mixtures' data points serve as the test dataset to test the prediction quality.

$$\%G_{mm,i} = \frac{h_{end}}{h_i} \times \frac{G_{mb}}{G_{mm}} \quad (10)$$

Where $\%G_{mm,i}$ means the $\%G_{mm}$ of the specimen at *i*th gyration; h_{end} means the height of the specimen when compaction ended; h_i is the specimen height at i^{th} gyration; G_{mb} is the bulk specific gravity of the specimen when the compaction ended; and G_{mm} is the maximum specific gravity of the asphalt mixture.

MACHINE LEARNING MODEL

Three machine-learning models will be built for different purposes and applications. These models are: (1) binary classification model, which is to select the appropriate input variables for the compaction prediction; (2) compaction classification model, which can predict the compaction condition and provide

information on different compaction categories based on the material density; and (3) density prediction model, which can predict the density value of the asphalt pavement.

Binary Classification Model

The SVM (support vector machine) was selected to build the binary classification model. It is a supervised machine-learning model for two-group classification problems. The purpose of the SVM is to find a plane that has the maximum margin (i.e., the maximum distance between data points of both classes) from the infinity of possible planes. If the original data can be separated linearly, the SVM would create a decision boundary (hyperplane) that can distinctly classify the N-dimensional data points [37]. If not, the SVM would create a new variable using the kernel function to move the original data to a higher dimension and do the nonlinear separation. The kernel function used in the SVM could be linear, polynomial, radial, etc. The data points that are closest to the hyperplane are the support vectors, which significantly influenced the position and orientation of the hyperplane. The SVM classifier is notable for its effectiveness in the high-dimensional data case, which is why it was selected in this study for the compaction prediction. The output of the SVM is two categories of compaction conditions: "Compaction Needed" and "Compaction Done." The selection of the density threshold (92% Gmm in this research) is based on the construction specification of PennDOT, which requires that the density of all 9.5-mm, 12.5-mm, 19-mm, and 25-mm wearing or binder courses be greater than 92% Gmm [38].

- Compaction Needed: The mixture with the $\%G_{mm}$ is smaller than 92%.
- Compaction Done: The mixture with the $\%G_{mm}$ is greater than 92%.

An SVM model is established to select the most suitable input variables for the compaction prediction. A total of 240 compaction data points from the same asphalt mixture (No. 1 in Table 1) were used for pre-modeling. Since only one mixture was used, the mixture designs were not necessarily involved in the model. Five different models were established, and the prediction errors and accuracy are shown in Table 7. The errors and prediction came from Scenario I, where all data points served as the training dataset.

Table 7. Pre-model results for input variables selection.

No.	Input	Errors	Accuracy (%)
1	CFI + Temp	31/240	87.08
2	CFI + Rotation + Temp	16/240	93.33
3	Rotation + Temp	17/240	92.92
4	NSI + Rotation + Temp	2/240	99.17
5	Energy + Rotation	3/240	98.75

Note: Temp is the compaction temperature. Rotation is the particle rotation during compaction. Energy is the accumulated compaction energy applied by the various compactors.

Models No. 4 and No. 5 both presented great prediction accuracy, which indicated that the combination of the NSI, particle rotation, temperature, and combination of compaction energy and particle rotation are the desirable input variables for compaction prediction. For Input No. 4, the normalized shearing index (NSI) can be easily monitored and collected by the gyratory compactor. However, the shearing resistances of the particulate materials are impractical to collect. The temperature in Table 7 is the sensor temperature instead of the material temperature. The temperature inside the sensor is a bit lagging compared to the temperature of the material because of the isolation of the sensor shell. Comparably, the compaction energy can be determined by the weight and vibration information of the roller compactors. Therefore, Model No. 5 was selected as the input for the compaction prediction. If more types of asphalt mixtures are included in

the model, the mixture design variables, such as the gradation and viscosity of the asphalt binder, should also be considered when evaluating the mixture's compactability. Eventually, the inputs of the machine learning model include:

(1) particle kinematic behavior, which is the relative rotation.
(2) accumulated compaction energy per unit mass
(3) mixture design information, which includes the mixture type, gradation, binder, etc.

Compaction Classification Model

Based on binary prediction experiences and the multicategory classification condition, multinomial logistic regression (MLR) was selected as the machine learning algorithm for the compaction classification model [39]. It is an extension of binary logistic regression that allows for more than two categories of the dependent variable. Binary logistic regression models a relationship between predictor variables and a categorical response variable. It is an extension of the linear regression model for classification problems. LR gives the probability between 0 and 1 based on the sigmoid function as presented in Equation 11 [40]. To predict which class a unit of data belongs to, a possibility threshold would be set. Like binary logistic regression, MLR uses maximum likelihood estimation to evaluate the probability of categorical membership. In the multicategory prediction, a reference category is selected, and a series of binary logistic regressions would be performed for the remaining categories to determine which class the data belongs to. One of the most significant advantages of logistic regression is that it is not only a classification model but also gives probabilities for each prediction. Knowing the likelihood of an event can offer more insights than the classification alone.

$$P(x) = \frac{1}{1+e^{-(\sum \beta_i x + \beta_0)}} \quad (11)$$

Different categories of compaction conditions of the asphalt mixture/pavement will be the output of the compaction classification model. The outputs of the model are five groups of compaction conditions in terms of the volumetric property: "Far under compaction," "Under compaction," "Good compaction," "High-density compaction," and "Over compaction." The determination of the threshold is based on the construction specification of PennDOT with the Percent Within Limits (PWL) [38]. The threshold in real practice is adjustable to the agency's requirements. Two predictive levels are considered in the paper, (1) classification with a fixed threshold value based on the %Gmm and (2) classification with a buffer zone. Details of these two predictive levels are explained in Table 8 and below.

(1) Classification with a fixed threshold value:

- Far under compaction (Class 1): The mixture with the $\%G_{mm}$ is less than 88%.
- Under compaction (Class 2): The mixture with the $\%G_{mm}$ is between 88% and 91%.
- Good compaction (Class 3): The mixture with the $\%G_{mm}$ is between 91% and 93%.
- High-density compaction (class 4): The mixture with the $\%G_{mm}$ is between 93% and 96%.
- Over compaction (Class 5): The mixture with the $\%G_{mm}$ is greater than 96%.

(2) Classification with a buffer zone:

- Compaction category: The $\%G_{mm}$ of the asphalt mixture that is beyond the $\pm 0.5\%G_{mm}$ of the threshold must be classified to the corresponding category.
- Buffer Zone: The $\%G_{mm}$ of the asphalt mixture that is within the $\pm 0.5\%G_{mm}$ of the threshold is acceptable to be classified in either neighbor category.

Table 8. Output category and density for the compaction classification model.

1	Far under compaction	< 88%G_{mm}
2	Under compaction	88%-91% G_{mm}
3	Good compaction	91%-93% G_{mm}
4	High-density compaction	93%-96% G_{mm}
5	Over compaction	> 96%G_{mm}

In MLR modeling, 11 asphalt mixtures, a total of 32 specimens with 4,154 compaction points, are used to build the prediction model. Because of the limited paper space, only partial data are displayed in Table 9. The first 7 columns of data serve as the inputs. The column "target" serves as the output for the model; 1~5 here represents the "Class 1~5" in terms of their volumetric property. The column "$\%G_{mm}$" is for determining the compaction condition (i.e., the column "target"). Based on the $\%G_{mm}$ of specimen at each gyration, 364 data points are categorized as "Far under compaction" (class 1), 342 data points are categorized as "Under compaction" (class 2), 439 data points are categorized as "Good compaction" (class 3), 1,316 data points and 1,693 data points are categorized to "High-density compaction" (class 4) and "Over compaction" (class 5), respectively.

Density Prediction Model

Artificial neural network (ANN) is one of the fastest-growing artificial intelligence (AI) techniques [41]. It is inspired by an animal's central nervous system and intended to simulate the behavior of biological systems composed of "neurons." For the advancements in data science and computing capacity, ANN has been applied to process complex problems in pavement construction and performance prediction [42, 43]. A neural network usually contains the input layer, hidden layers, and output layer, as shown in Figure 25. The input and output layer are to feed raw information into the network and provide the prediction from the algorithm. The hidden layer connects the input and output and determines the activity of each hidden unit by calculation algorithms [41].

Table 9. Partial data of the compaction predictive model.

Type	Additive	NMSA	Binder	Rotation (x)	Rotation (y)	Energy	Target	$\%G_{mm}$
1	0	9.5	76	1.176	1.493	140.0	1	84.16
1	0	9.5	76	1.193	1.491	155.4	1	84.74
1	0	9.5	76	1.169	1.499	170.7	1	85.26
1	0	9.5	76	1.126	1.461	185.8	1	85.73
1	0	9.5	76	1.121	1.500	201.0	1	86.19
1	0	9.5	76	1.146	1.170	363.0	2	89.48
1	0	9.5	76	1.163	1.168	377.5	2	89.70
1	0	9.5	76	1.155	1.100	392.0	2	89.91
1	0	9.5	76	1.154	1.112	406.3	2	90.06
1	0	9.5	76	1.169	1.088	420.8	2	90.28
1	0	9.5	76	1.140	0.907	620.9	3	92.24
1	0	9.5	76	1.150	0.895	635.4	3	92.40
1	0	9.5	76	1.149	0.894	649.7	3	92.48
1	0	9.5	76	1.157	0.893	663.9	3	92.55
1	0	9.5	76	1.145	0.871	678.5	3	92.71
1	0	9.5	76	1.143	0.890	692.8	3	92.79
1	0	9.5	76	1.151	0.827	807.1	4	93.49
1	0	9.5	76	1.139	0.812	821.4	4	93.57
1	0	9.5	76	1.149	0.804	835.6	4	93.65
1	0	9.5	76	1.138	0.788	849.8	4	93.73
1	0	9.5	76	1.118	0.807	864.0	4	93.81
1	0	9.5	76	1.125	0.791	878.2	4	93.89
1	0	9.5	76	1.127	0.803	892.4	4	93.97
1	0	9.5	76	1.108	0.767	906.6	4	94.05
1	0	9.5	76	0.682	0.981	1,511.9	5	96.10
1	0	9.5	76	0.667	1.002	1,526.1	5	96.18
1	0	9.5	76	0.656	0.993	1,540.1	5	96.18
1	0	9.5	76	0.652	0.979	1,554.3	5	96.26
1	0	9.5	76	0.656	0.980	1,568.3	5	96.26
1	0	9.5	76	0.646	0.989	1,582.2	5	96.26
1	0	9.5	76	0.627	0.981	1,596.4	5	96.35
1	0	9.5	76	0.661	0.990	1,610.3	5	96.35

Note: "Type" represents the type of asphalt mixture. 0 is the HMA, and 1 is the WMA. "NMAS" is the nominal maximum aggregate size, and the "Binder" is the high-temperature performance grade of the virgin binder. "Energy" is the accumulated compaction energies that are applied to the material from the beginning.

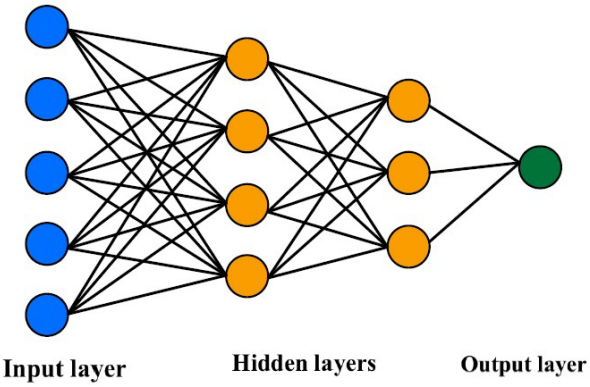

Figure 26. Configuration of the artificial neural network.

In ANN modeling, the same 11 asphalt mixtures and 4,154 compaction points are used to establish the prediction model. Like the MLR modeling, the First 7 columns in Table 9 serve as the inputs, which means 7 neurons in the input layer. The column "*%Gmm*" serves as the output for the model. The predictive quality can be obtained by comparing the specimen density with the ANN prediction results.

CHAPTER 6

Compaction Prediction

The prediction results of the compaction classification model and the density prediction model will be presented in this section. The models are built and calibrated by the lab compaction data, then used for the field compaction prediction. The 4,154 compaction points from the gyratory compaction are used for the model establishment and calibration; 2 field project data are adopted for model verification.

COMPACTION CLASSIFICATION MODEL

Laboratory Compaction Prediction

The MLR model is established and calibrated by the lab compaction data. Considering the imbalanced distribution of the classification categories, sensitivity, specificity, and accuracy are calculated to evaluate the prediction quality. The calculations of three metrics are presented in Table 10 and Equations 12–14.

Table 10. Prediction configuration of the MLR model.

Prediction (Model)	Reference ($\%G_{mm}$) Class 1	Reference ($\%G_{mm}$) Class 2	Reference ($\%G_{mm}$) Class 3	Reference ($\%G_{mm}$) Class 4	Reference ($\%G_{mm}$) Class 5
Class 1	True (A11)	False (A12)	False (A13)	False (A14)	False (A15)
Class 2	False (A21)	True (A22)	False (A23)	False (A24)	False (A25)
Class 3	False (A31)	False (A32)	True (A33)	False (A34)	False (A35)
Class 4	False (A41)	False (A42)	False (A43)	True (A44)	False (A45)
Class 5	False (A51)	False (A52)	False (A53)	False (A54)	True (A55)

$$Sensitivity\ of\ Class\ k = {A_{kk}}\Big/{\sum_{i=1}^{5} A_{ik}} \tag{12}$$

$$Specificity\ of\ Class\ k = {\left(\sum_{i=1}^{5} A_{ii} - A_{kk}\right)}\Big/{\left(\sum_{i=1}^{5}\sum_{j=1}^{5} A_{ij} - \sum_{i=1}^{5} A_{ik}\right)} \tag{13}$$

$$Accuracy = {\sum_{i=1}^{5} A_{ii}}\Big/{\sum_{i=1}^{5}\sum_{j=1}^{5} A_{ij}} \tag{14}$$

The prediction results of the MLR model under different scenarios are shown in Table 11. Most predictions have more than 90% accuracy when fixed thresholds are used for prediction. Errors are greatly reduced when the buffer zone is set, indicating that most of the errors occur near the thresholds. For scenarios II and III, in which the test dataset is different from the corresponding training dataset, satisfactory prediction quality is also achieved. That reveals the robustness of the MLR model for the compaction prediction and the appropriate selection for the input variables. Conclusively, the intelligent method using

a machine learning algorithm is a practical method to predict the compaction condition of the asphalt specimen in the lab.

Table 11. Lab compaction prediction for the MLR model.

Scenario/Parameters		Class 1	Class 2	Class 3	Class 4	Class 5
		No buffer zone	**No buffer zone**	**No buffer zone**	**No buffer zone**	**No buffer zone**
I	Accuracy (error)	92.87% (296/ 4,154)	92.87% (296/ 4,154)	92.87% (296/ 4,154)	92.87% (296/ 4,154)	92.87% (296/ 4,154)
	Sensitivity (%)	96.15	89.77	88.16	91.57	95.04
	Specificity (%)	99.60	99.16	98.55	95.84	96.87
II	Accuracy (error)	93.58% (80/ 1,247)	93.58% (80/ 1,247)	93.58% (80/ 1,247)	93.58% (80/ 1,247)	93.58% (80/ 1,247)
	Sensitivity (%)	97.98	88.54	91.20	93.47	94.30
	Specificity (%)	99.39	99.48	98.66	95.60	98.01
III	Accuracy (error)	91.75% (119/ 1,442)	91.75% (119/ 1,442)	91.75% (119/ 1,442)	91.75% (119/ 1,442)	91.75% (119/ 1,442)
	Sensitivity (%)	97.96	88.64	86.98	85.91	98.55
	Specificity (%)	99.07	98.63	98.98	98.50	93.53
		Buffer zone setup	**Buffer zone setup**	**Buffer zone setup**	**Buffer zone setup**	**Buffer zone setup**
I	Accuracy (error)	99.64% (15/ 4,154)	99.64% (15/ 4,154)	99.64% (15/ 4,154)	99.64% (15/ 4,154)	99.64% (15/ 4,154)
	Sensitivity (%)	99.18	98.54	99.77	99.77	99.82
	Specificity (%)	99.68	99.74	99.62	99.58	99.51
II	Accuracy (error)	99.76% (3/1,247)	99.76% (3/1,247)	99.76% (3/1,247)	99.76% (3/1,247)	99.76% (3/1,247)
	Sensitivity (%)	100	99.42	100	100	99.94
	Specificity (%)	99.92	99.97	99.92	99.89	99.92
III	Accuracy (error)	99.38% (9/1,442)	99.38% (9/1,442	99.38% (9/1,442	99.38% (9/1,442	99.38% (9/1,442
	Sensitivity (%)	100	98.83	99.77	99.70	100
	Specificity (%)	99.76	99.87	99.78	99.82	99.63

Field Compaction Prediction

As elaborated in Figures 17 and 18, the lab compaction and field compaction can be connected by the particle kinematic behavior (particle rotation) during compaction, which is the basis of developing the field compaction monitoring method. As shown in Equation 15, the Pearson correlation coefficient was calculated based on the average particle rotation under the same amount of compaction energies for two compactions. The Pearson correlation coefficient is 0.806, which means the high correlation between the gyratory and roller compaction.

$$r = \frac{\sum (x_i - \bar{x})(y_i - \bar{y})}{\sqrt{\sum (x_i - \bar{x})^2 \sum (y_i - \bar{y})^2}} \quad (15)$$

Where ***r*** is the Pearson correlation coefficient; ***xi*** is the particle rotation under gyratory compaction; $\overline{x}$ is the mean of the *x* sample; ***yi*** is the particle rotation under roller compaction; $\overline{y}$ is the mean of the *y* sample.

Given the high correlation between the gyratory and roller compaction, it is reasonable to predict the field compaction condition using the intelligent model trained by the lab data. The input information and the prediction results of the two field projects are presented in Table 12. These two projects use different asphalt mixtures and pavement structures and different roller compaction patterns. For the Altoona project, a total of 11 compaction cycles were applied. It is noted that the "Far under compaction" category is predicted at the beginning for its limited energy and large particle rotations. The skeleton then forms as more energy is applied, which hinders the rotation of the internal particles, hence the "Under compaction" is predicted. The compaction eventually enters the "Good compaction" category when enough energy is used, and stable particle rotation is achieved. Two pavement cores near the SmartRock sensor are taken out to check the density, which is 93.1% Gmm and 93.6% Gmm, which is at the buffer zone between the "Good compaction" and "High density compaction" categories.

For the Indiana project, two vibratory compactions and one pass of static compaction were applied. The last cycle of static compaction is missing due to technical reasons. Based on the compaction experiences, the static compaction at the end serves more like leveling and limited densification is achieved. Table 12 indicates that the compaction has entered the "Under compaction" category when the first vibration is applied. The pavement is predicted to the "Good compaction" after the two vibratory cycles. Two pavement cores are drilled out to check the density after compaction. The density of the core samples near the SmartRock is 92.8% G_{mm} and 92.5% G_{mm}, which is in the volumetric range of the "Good compaction" category. Two field projects verified that it is practical and promising to predict pavement compactability by the machine learning algorithm. The particle rotation of the lab compaction could be used to predict the field compaction condition if the intelligent model was appropriately trained.

Table 12. Field compaction prediction based on the MLR model.

Type	Additive	NMSA	Binder	Rotation (x)	Rotation (y)	Energy	Roller	Prediction
Altoona Project								
1	0	9.5	76	3.03	1.15	77.9	V	Class 1
1	0	9.5	76	1.45	0.44	155.9	V	Class 1
1	0	9.5	76	0.10	0.96	233.8	V	Class 1
1	0	9.5	76	0.55	0.43	298.4	S	Class 1
1	0	9.5	76	0.66	0.46	363.1	S	Class 2
1	0	9.5	76	1.10	0.48	427.7	S	Class 2
1	0	9.5	76	1.00	1.30	505.7	V	Class 2
1	0	9.5	76	0.03	0.08	583.6	V	Class 3
1	0	9.5	76	0.56	0.20	661.6	V	Class 3
1	0	9.5	76	0.41	0.42	697.5	S	Class 3
1	0	9.5	76	0.18	0.36	733.4	S	Class 3
Indiana Project								
0	0	12.5	64	8.17	2.05	229.7	V	Class 2
0	0	12.5	64	3.59	1.04	459.4	V	Class 3

Note: Roller "V" and "C" mean vibratory and static roller compaction; Class "1," "2," and "3" represent "Far under compaction", "Under compaction" and "Good compaction", respectively.

DENSITY PREDICTION MODEL

Laboratory Compaction Prediction

Another prediction model, the density prediction model, was built to predict the density value of the asphalt pavement. For the lab compaction, the specimen density can be obtained by the height of the specimen and the final density; the prediction quality of the model can thus be quantified by comparing the density of the SGC measurement and the prediction from the ANN model. The mean relative error (MRE) and root mean square error (RMSE) are used for the prediction evaluation. Their calculations are as shown in Equations 16 and 17. Typically, the larger value of the MRE and larger value of RMSE indicate more variation between the prediction and true value, and thus lower prediction accuracy.

$$MRE = \frac{1}{n}\sum_{i=1}^{n}\frac{|Y_i - X_i|}{X_i} \times 100\% \quad (16)$$

$$RMSE = \sqrt{\frac{1}{n}\sum_{i=1}^{n}(Y_i - X_i)^2} \quad (17)$$

Where $\boldsymbol{Y_i}$ is the predictive density at the *i*th measurement; $\boldsymbol{X_i}$ is the specimen density at the *i*th measurement. $\boldsymbol{n}$ is the number of measurements.

Based on the experiences of the ANN modeling, two hidden layers can handle most prediction problems at a high processing efficiency and also avoid overfitting [44]. The number of neurons hidden can be selected between the numbers of input and output neurons [44]. Therefore, several configurations of ANN models are built as shown in Table 13 to test the prediction accuracy. To clarify, the number series 7-6-5-1 means the number of neurons in the input layer, (first and second) hidden layer, and output layer. Configurations 7-5-3-1, 7-5-2-1, and 7-4-2-1 cannot converge the prediction at the set numbers of steps because of the inefficient calculation; their results are not presented in the table. Eventually, the configuration of 7-6-3-1 is selected based on its smallest RMSE and MRE.

Table 13. Prediction comparison for different ANN configurations.

Configuration of ANN	RMSE	MRE (%)
7-6-5-1	0.3743	0.2987
7-6-4-1	0.3741	0.3054
7-6-3-1	0.3649	0.2954
7-6-2-1	0.3752	0.3013
7-5-4-1	0.3788	0.3072
7-4-3-1	0.3718	0.3037

The prediction results of the MLR model under different scenarios are shown in Figures 27–29 and Table 14. All of the prediction errors are smaller than 1% MRE and 0.5 RMSE. The satisfactory prediction quality is also achieved even for Scenarios II and III in which the test dataset is different from the corresponding training dataset. These results affirm the appropriate selection for the input variables and the robustness of the ANN model for the compaction prediction.

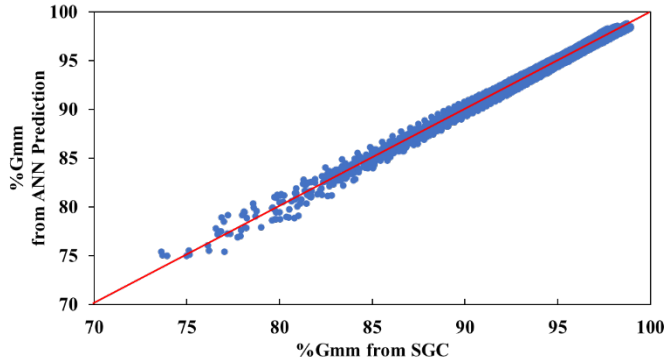

Figure 27. Comparison between the specimen density and ANN prediction for Scenario I.

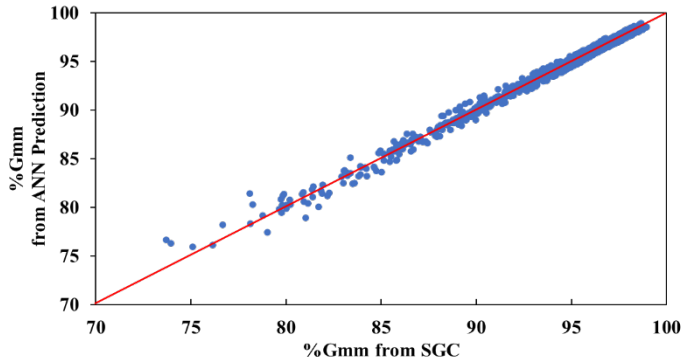

Figure 28. Comparison between the specimen density and ANN prediction for Scenario II.

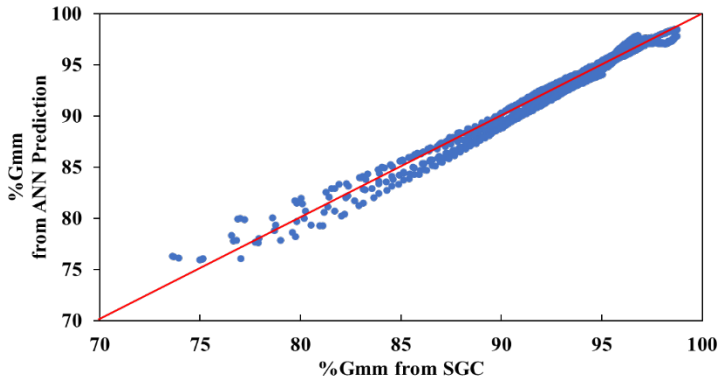

Figure 29. Comparison between the specimen density and ANN prediction for Scenario III.

Table 14. Prediction of ANN model for different data scenarios.

Scenario	Training	Testing	RMSE	MRE (%)
I	All data points	All data points	0.26	0.32
II	70% random data points	Rest 30% of data points	0.30	0.39
III	8 mixtures of data points	Rest 3 mixtures data points	0.48	0.60

Field Compaction Prediction

The prediction results of the two field projects by the density prediction model are shown in Table 15. It is noticed that reasonable density has been predicted from the beginning to the end of the compaction for both field projects, even though the numbers of compaction cycles, pavement structure, and materials are different. The cores were drilled from both projects at the end of the compaction, and the density of the pavement cores is presented in Table 15. For the Altoona project, the density near the SmartRock is 93.1% and 93.6% Gmm, which is close to the prediction, 93.1% Gmm. For the Indiana project, the density near the SmartRock is 92.5% and 92.8% Gmm, which is also close to the prediction, 93.1% Gmm. The prediction errors for both projects are within 0.5% MRE, which further confirms the practicality and feasibility of the ANN model to predict the density of the asphalt pavement. The concept of using the lab compaction data to predict the density in the field is also workable.

Table 15. Field compaction prediction based on the ANN model.

Project	**Altoona Project**										
Cycle	1	2	3	4	5	6	7	8	9	10	11
Roller	V	V	V	S	S	S	V	V	V	S	S
ANN	78.2	83.7	88.3	88.8	89.8	90.3	91..4	92.2	92.4	92.8	93.1

Project	**Indiana**	
Cycle	1	2
Roller	V	V
ANN	91.7	93.1

Note:
Core density is the density of the core sample (%*Gmm*) for verification.
Core density for Altoona Project is **93.1%, 93.6% G_{mm}.**
Core density for Indiana Project is **92.5% and 92.8% G_{mm}.**

CHAPTER 7

Conclusions and Future Work

This project focuses on the compaction of infrastructure materials, mainly asphalt mixtures and granular materials. It aims to investigate the compaction mechanism and develop an intelligent compaction monitoring system to predict the density of asphalt pavement. Several lab experiments and field projects have been conducted to study particle kinematic behaviors under various compactions. After understanding the particle behaviors under the compaction loadings, a novel compaction monitoring system is established and calibrated by the laboratory compaction data to predict the density of field asphalt pavement. Several findings have been discovered.

(1) The design of the roller compaction would affect the particle kinematic behaviors during compaction. Static compaction contributes limited densification to the asphalt pavement, especially applied after the vibratory compaction. The vibratory compaction response is more associated with the material's density and not affected by the compaction sequence pattern, which makes the vibratory response an appropriate parameter to evaluate the compactability of the asphalt pavement.

(2) Similar three-stage compaction patterns are identified for both lab and field compaction in terms of particle rotation in the horizontal direction: breakdown stage, main compaction stage, and finishing stage. Different compaction stages are related to the material's properties and the interactions between the compaction loadings and particle shearing resistances. The largest particle rotation occurs in the breakdown stage. The main compaction stage is characterized as the imbalanced interaction between the compaction loadings and particle shearing resistance. The finishing stage produces more leveling/smoothing effect than compaction, since only minimal densification occurs in this stage.

(3) The ICMV is calculated based on the IC theory, which collects the external responses from the entire pavement structure by the accelerometer on the vibratory roller. No specific correlations are found between the ICMV from the roller compactor and the particle acceleration from the internal asphalt material layer. It is recommended to evaluate the compactablity of asphalt pavement by jointly considering the internal and external responses during compaction.

(4) The particle-size wireless sensor, SmartRock, was used in the project to collect the particle kinematic behaviors during compaction, such as particle rotation, acceleration, etc. These parameters are related to the compactability of the materials and are used for density evaluation and prediction. The SmartRock sensor is an appropriate microelectromechanical systems (MEMS) device to realize smart compaction.

(5) A modified version of the logistic regression, multinominal logistic regression (MLR), is applied to classify the compaction condition of the asphalt pavement. An artificial neural network (ANN) model is developed to predict the density of the asphalt pavement. The prediction results show that both the compaction classification model and the density prediction model are appropriate and promising to predict the compaction conditions of asphalt pavement using the particle rotation, compaction energy, and mixture design information as the input variables.

(6) Two field compaction projects have been conducted to verify the robustness of the compaction prediction models. Although the model is built and calibrated only by the lab compaction data,

reasonable compaction density conditions are predicted for both projects. It is noted that these two projects used different materials under distinct pavement structures and compaction patterns. The results confirm that the lab and field compaction can be reasonably connected by particle rotation and using the lab data to predict the field compaction conditions is feasible.

(7) The quality control of asphalt pavement compaction is affected by many factors. The results and conclusions in this study are based on the 11 asphalt mixtures in the lab compaction and 3 field projects, which is far from enough. Future studies and simulations that include more types of asphalt mixtures, compaction designs, and pavement structures are recommended to assess the concept of the compaction mechanisms and evaluate the robustness of the compaction models.

(8) This project applies a SmartRock sensor to monitor and predict the compaction condition and density of the asphalt pavement. The sensor application could be limited to localized spots and be challenging to achieve full coverage. Considering the advantages of the IC technology with full pavement coverage, integrating the smart compaction monitoring system and the IC technology could be promising in the future to achieve a more advanced compaction monitoring program for asphalt pavement construction.

Acknowledgment

This project was funded by the USDOT Region 3 University Transportation Center (UTC), Center for Integrated Asset Management for Multimodal Transportation Infrastructure Systems (CIAMTIS). The research team would like to thank Railroad Technology and Services, LLC (RTS) for providing the SmartRock sensors and technical support. Special thanks go to Mr. Richard Steger from Ingevity Corporation, Mr. Kevin Gnegy from Pennsylvania DOT, Mr. Mark Moyer from New Enterprise Stone & Lime Co. Inc., and Mr. Jeff Austin from Brooks Construction for supporting field and laboratory tests.

References

1. Sadasivam, S. (2004). *Evaluation of the Effects of Compaction Methods on the Predicted Performance of Superpave Mixtures*. Doctoral Dissertation, North Carolina State University: Raleigh, NC, p. 155.
2. Lindenand, R.N., J.P. Mahoney, and N.C. Jackson (1989). Effect of Compaction on Asphalt Concrete Performance. *Transportation Research Record, 1217*, 20-28.
3. Meehan, C., D. Cacciola, F. Tehrani, and W.J. Baker III (2016). Assessing soil compaction using continuous compaction control and location-specific in situ tests. *Automation in Construction, 73*. https://doi.org/10.1016/j.autcon.2016.08.017
4. Wang, X., S. Shen, H. Huang, and L.C. Almeida (2018). Characterization of particle movement in Superpave gyratory compactor at mesoscale using SmartRock sensors. *Construction and Building Materials, 175*, 206-214. https://doi.org/https://doi.org/10.1016/j.conbuildmat.2018.04.146
5. Zheng, J.-L., X. Chen, Q.-R. Li, R.-H. Ying (2008). ANSYS research on the vibratory compacting process of hot asphalt mixture pavement. *Engineering Mechanics, 25*(10), 200-206.
6. Federal Highway Administration (2013). *Intelligent Compaction*. TechBrief, FHWA-HIF-13-051.
7. Chang, G.K., Q. Xu, J.L. Rutledge, and S. Garber (2014). *A Study on Intelligent Compacting and In-Place Asphalt Density*, Report No. FHWA-HIF-14-017.
8. Hu, W., X. Jia, B. Huang, and H. Park (2017). Evaluation of compactability of asphalt mixture utilizing asphalt vibratory compactor. *Construction and Building Materials, 139*, 419-429. https://doi.org/https://doi.org/10.1016/j.conbuildmat.2017.02.070
9. Zhang, C., and A. Elaksher (2012). *An Unmanned Aerial Vehicle-Based Imaging System for 3D Measurement of Unpaved Road Surface Distresses*, Wiley Online Library [https://doi.org/10.1111/j.1467-8667.2011.00727.x]. *Computer-Aided Civil and Infrastructure Engineering, 27*(2), 118-129. https://doi.org/https://doi.org/10.1111/j.1467-8667.2011.00727.x
10. De Maeijer, P.K., G. Luyckx, C. Vuye, and E. Voet (2019). Fiber Optics Sensors in Asphalt Pavement: State-of-the-Art Review. *Infrastructures*, *4*(2), DOI: 10.3390/infrastructures4020036.
11. Plati, C., A. Loizos (2012). Using ground-penetrating radar for assessing the structural needs of asphalt pavements. *Nondestructive Testing and Evaluation, 27*(3), 273-284. https://doi.org/10.1080/10589759.2012.695784
12. Seraj, F., B.J. van der Zwaag, A. Dilo, T. Luarasi, and P. Havinga (2016). RoADS: A Road Pavement Monitoring System for Anomaly Detection Using Smart Phones. In *Big Data Analytics in the Social and Ubiquitous Context*. Cham: Springer International Publishing.
13. Wang, X., S. Shen, H. Huang, and Z. Zhang (2019). Towards smart compaction: Particle movement characteristics from laboratory to the field. *Construction and Building Materials, 218*, 323-332. https://doi.org/10.1016/j.conbuildmat.2019.05.122
14. Wang, N., F. Chen, T. Ma, Y. Luan, and J. Zhu (2022). Compaction performance of cold recycled asphalt mixture using SmartRock sensor. *Automation in Construction, 140*, 104377. https://doi.org/https://doi.org/10.1016/j.autcon.2022.104377
15. Yu, S., S. Shen, R. Steger, and X. Wang (2022). Effect of warm mix asphalt additive on the workability of asphalt mixture: From particle perspective. *Construction and Building Materials, 360*, 129548. https://doi.org/https://doi.org/10.1016/j.conbuildmat.2022.129548

16. Cheng, Z., D. Zhang, S. Xie, and P. Polaczyk (2022). SmartRock-Based Research on Gyratory Locking Point for Stone Mastic Asphalt Mixture. *Buildings, 12*(2), 97. https://doi.org/https://doi.org/10.3390/buildings12020097
17. Zhang, D., Z. Cheng, D. Geng, and S. Xie (2022). Experimental and Numerical Analysis on Mesoscale Mechanical Behavior of Coarse Aggregates in the Asphalt Mixture during Gyratory Compaction. *Processes, 10*(1), 47. https://doi.org/https://doi.org/10.3390/pr10010047
18. Polaczyk, P., B. Han, B. Huang, X. Jia, and X. Shu (2018). Evaluation of the hot mix asphalt compactability utilizing the impact compaction method. *Construction and Building Materials, 187*, 131-137. https://doi.org/10.1016/j.conbuildmat.2018.07.117
19. Souza, V.M.A., R. Giusti, and A.J.L. Batista. (2018). Asfault: A low-cost system to evaluate pavement conditions in real-time using smartphones and machine learning. *Pervasive and Mobile Computing, 51*, 121-137. https://doi.org/https://doi.org/10.1016/j.pmcj.2018.10.008
20. Nabipour, N., N. Karballaeezadeh, A. Dineva, and A. Mosavi (2019). Comparative Analysis of Machine Learning Models for Prediction of Remaining Service Life of Flexible Pavement. *Mathematics, 7*(1198). https://doi.org/doi:10.3390/math7121198
21. Marcelino, P., M. de Lurdes Antunes, E. Fortunato, and M. Castilho Gomes (2021). Machine learning approach for pavement performance prediction. *International Journal of Pavement Engineering, 22*(3), 341-354. https://doi.org/10.1080/10298436.2019.1609673
22. Kwigizileand, V., R.N. Mussa, and M. Selekwa (2005). Connectionist Approach to Improving Highway Vehicle Classification Schemes: The Florida Case. *Transportation Research Record, 1917*(1), 182-189. https://doi.org/10.1177/0361198105191700120
23. Amorim, S.I.R., J.C. Pais, A.C. Vale, and M.J.C. Minhoto (2015). A model for equivalent axle load factors. *International Journal of Pavement Engineering, 16*(10), 881-893. https://doi.org/10.1080/10298436.2014.968570
24. Zhang, C., S. Shen, H. Huang, and L. Wang (2021). Estimation of the Vehicle Speed Using Cross-Correlation Algorithms and MEMS Wireless Sensors. *Sensors (Basel, Switzerland), 21*(5), 1721. https://doi.org/10.3390/s21051721
25. Eleyedath, A., and A.K. Swamy (2020). Prediction of dynamic modulus of asphalt concrete using hybrid machine learning technique. *International Journal of Pavement Engineering*, *23*(6):2083-2098. https://doi.org/10.1080/10298436.2020.1841191
26. Behnood, A., E. M. Golafshani. (2021). Predicting the dynamic modulus of asphalt mixture using machine learning techniques: An application of multi biogeography-based programming. *Construction and Building Materials, 266*(A), 120983. https://doi.org/https://doi.org/10.1016/j.conbuildmat.2020.120983
27. Liu, S., H. Huang, T. Qiu, and J. Kwon (2016). Effect of geogrid on railroad ballast particle movement. *Transportation Geotechnics, 9*, 110-122. https://doi.org/https://doi.org/10.1016/j.trgeo.2016.08.003
28. Liu, S., H. Huang, and T. Qiu (2017). Comparison of Laboratory Testing Using SmartRock and Discrete Element Modeling of Ballast Particle Movement. *Journal of Materials in Civil Engineering, 29*(3), D6016001. https://doi.org/10.1061/(ASCE)MT.1943-5533.0001540
29. Pillitteri, S., G. Lumay, E. Opsomer, N. Vandewalle (2019). From jamming to fast compaction dynamics in granular binary mixtures. *Scientific Reports, 9*(1), 7281. https://doi.org/10.1038/s41598-019-43519-6
30. Wang, X., H. Huang, E. Tutumluer, and S. Shen (2022). Monitoring Particle Movement under Compaction using SmartRock Sensor: A Case Study of Granular Base Layer Compaction. *Transportation Geotechnics, 34*, 100764. https://doi.org/10.1016/j.trgeo.2022.100764
31. Anderegg, R., and K. Kaufmann (2004). Intelligent Compaction with Vibratory Rollers: Feedback Control Systems in Automatic Compaction and Compaction Control. *Transportation Research Record, 1868*(1), 124-134. https://doi.org/10.3141/1868-13

32. Manzi, S., C. Mazzotti, and M.C. Bignozzi. (2017). Self-compacting concrete with recycled concrete aggregate: Study of the long-term properties. *Construction and Building Materials, 157*, 582-590. https://doi.org/https://doi.org/10.1016/j.conbuildmat.2017.09.129
33. Mahmoud, A.F.F., and H.U. Bahia (2004). *Using gyratory compactor to measure mechanical stability of asphalt mixtures*. Wisconsin Highway Research Program, Report No. WHRP 05-02.
34. DelRio-Prat, M., A. Vega-Zamanillo, D. Castro-Fresno, and M.Á. Calzada-Pérez (2011). Energy consumption during compaction with a Gyratory Intensive Compactor Tester. Estimation models. *Construction and Building Materials, 25*(2), 979-986. https://doi.org/https://doi.org/10.1016/j.conbuildmat.2010.06.083
35. Liu, D., M. Lin, and S. Li. (2016). Real-Time Quality Monitoring and Control of Highway Compaction. *Automation in Construction, 62*, 114-123. https://doi.org/https://doi.org/10.1016/j.autcon.2015.11.007
36. Zhao, Y., S. Xie, Y. Gao, Y. Zhang and K. Zhang (2021). Prediction of the number of roller passes and degree of compaction of asphalt layer based on compaction energy. *Construction and Building Materials, 277*, 122274. https://doi.org/https://doi.org/10.1016/j.conbuildmat.2021.122274
37. Cervantes, J., F. Garcia-Lamont, L. Rodríguez-Mazahua, and A. Lopez (2020). A comprehensive survey on support vector machine classification: Applications, challenges and trends. *Neurocomputing, 408*, 189-215. https://doi.org/https://doi.org/10.1016/j.neucom.2019.10.118
38. Pennsylvania Department of Transportation, Specification, in *Publication 408/2020*. 2020: Harrisburg, PA.
39. Yu, S., and S. Shen. (2022). Compaction Prediction for Asphalt Mixtures Using Wireless Sensor and Machine Learning Algorithm. *IEEE Transactions on Intelligent Transportation Systems*, *24*(1), 778-786. https://doi.org/10.1109/TITS.2022.3218692.
40. Montgomery, D.C., E.A. Peck, and G.G. Vining (2021). *Introduction to linear regression analysis* (sixth edition ed.). Hoboken John Wiley & Sons, Inc.
41. Moayedi, H., M. Mosallanezhad, A.S.A. Rashid, W.A.W. Jusoh and M.A. Muazu (2020). A systematic review and meta-analysis of artificial neural network application in geotechnical engineering: theory and applications. *Neural Computing and Applications, 32*(2), 495-518. https://doi.org/10.1007/s00521-019-04109-9
42. Hou, Y., Q. Li, C. Zhang, and G. Lu (2021). The State-of-the-Art Review on Applications of Intrusive Sensing, Image Processing Techniques, and Machine Learning Methods in Pavement Monitoring and Analysis. *Engineering, 7*(6), 845-856. https://doi.org/https://doi.org/10.1016/j.eng.2020.07.030
43. Yang, X., J. Guan, L. Ding, Z. You, V.C.S. Lee, M.R.M. Hasan, and X. Cheng (2021). Research and applications of artificial neural network in pavement engineering: A state-of-the-art review. *Journal of Traffic and Transportation Engineering (English Edition), 8*(6), 1000-1021. https://doi.org/https://doi.org/10.1016/j.jtte.2021.03.005
44. Malekian, A., and N. Chitsaz (2021). Concepts, procedures, and applications of artificial neural network models in streamflow forecasting. *Advances in Streamflow Forecasting: From Traditional to Modern Approaches, 25*, 115-147. https://doi.org/https://doi.org/10.1016/B978-0-12-820673-7.00003-2